An hp-Adaptive Pseudospectral Method for Solving Optimal Control Problems

Christopher L. Darby*
William W. Hager †
Anil V. Rao‡

University of Florida
Gainesville, FL 32611

Abstract

An hp-adaptive pseudospectral method is presented for numerically solving optimal control problems. The method presented in this paper iteratively determines both the number of segments, the width of each segment, and the polynomial degree required in each segment in order to obtain a solution to a user-specified accuracy. Starting with a global pseudospectral approximation for the state, on each iteration the method determines locations for the segment breaks and the polynomial degree in each segment for use on the next iteration. The number of segments and the degree of the polynomial on each segment continue to be updated until a user-specified tolerance is met. The terminology "hp" is used because the segment widths (denoted h) and the polynomial degree (denoted p) in each segment are determined simultaneously. It is found that the method developed in this paper leads to higher accuracy solutions with less computational effort and memory than is required in a global pseudospectral method. Consequently, the method makes it possible to solve complex optimal control problems using pseudospectral methods in cases where a global pseudospectral method would be computationally intractable. Finally, the utility of the method is demonstrated on a variety of problems of varying complexity.

1 Introduction

Over the past two decades, direct collocation methods have become popular in the numerical solution of nonlinear optimal control problems. In a direct collocation method, the state is approximated using a set of trial (basis) functions and the dynamics are collocated at specified set of points in the time interval. Most commonly, direct collocation methods for optimal control are employed using so called

*PhD Candidate. Department of Mechanical and Aerospace Engineering. E-mail: cdarby@ufl.edu.
†Professor. Department of Mathematics. E-mail: hager@ufl.edu.
‡Assistant Professor. Department of Mechanical and Aerospace Engineering. E-mail: anilvrao@ufl.edu. Corresponding Author.

h-methods where a fixed low-degree polynomial (e.g., third-degree or fourth-degree) state approximation is used and the problem is divided into segments. Convergence of the numerical discretization is then achieved by increasing the number of segments [1, 2, 3]. Grid refinement techniques are used largely on the goal of obtaining a specified solution accuracy by increasing the number of mesh intervals in regions of the trajectory where the errors are largest. Excellent examples of h-methods for solving optimal control problems are given in Refs. [4, 2, 3, 5, 6].

In recent years, the class of *pseudospectral methods* for solving optimal control problems has increased in popularity [7, 8, 9, 10, 11, 12, 13, 14, 15, 16]. In a pseudospectral method, the collocation points are chosen based on accurate quadrature rules and the basis functions are typically Chebyshev or Lagrange polynomials. In contrast to an h method, a pseudospectral method is typically employed as a p-method where a single segment is used, and convergence is achieved by increasing the degree p of the polynomial. For problems whose solutions are infinitely smooth and well-behaved, a pseudospectral method has a simple structure and converges spectrally [17, 18, 19] (i.e., at an exponential rate). The most well developed pseudospectral methods are the the *Gauss pseudospectral method* (GPM) [9, 10], the *Radau pseudospectral method* [14, 15, 16] (RPM), and the *Lobatto pseudospectral method* [7] (LPM).

While pseudospectral methods have typically been applied as p-methods [7, 8, 9, 10, 15, 16], relying on convergence using global polynomials has several limitations. For even many smooth problems an accurate approximation may be obtained only if a very large-degree global polynomial is used. In addition, many optimal control problems have either nonsmooth solutions or nonsmooth problem formulations. In these cases, the convergence rate of a p-method may be extremely slow, resulting in a poor approximation even if a very high degree polynomial is used. A second limitation of a p-method for solving optimal control problems is that the use of a high degree global polynomial results in a nonlinear programming problem (NLP) that has a constraint Jacobian and Hessian that grows in density and size much faster than the number of collocation points. As a result, while it may be possible to achieve convergence using a p-method, such an approach may be computationally intractable or inefficient due to the number of nonzero derivatives in the NLP. An alternative to implementing a pseudospectral method as a p-scheme is to use an h-type pseudospectral method [5, 6, 14]. It is noted, however, that an h-method may require using a large number of mesh intervals in order to achieve an acceptable error tolerance. Furthermore, because spectral accuracy is lost when using an h-type pseudospectral method, achieving a given accuracy may result in an extremely large NLP.

In order to increase the utility of pseudospectral methods while attempting to maintain as close to spectral accuracy as possible, in this paper we present a new *hp-adaptive pseudospectral method* that allows the number of segments, segment widths, and polynomial degrees to vary throughout the time

interval of interest. The method uses a two-tiered strategy to determine the locations of segments and the degree of the polynomial within a segment to achieve a specified solution accuracy. If the error across a particular segment has a uniform-type behavior, then the number of collocation points is increased. If the error at isolated points is significantly larger than errors at other points in a segment, then a segment is subdivided at these isolated points. The method described in this paper provides an accurate solution at the collocation points and also computes an accurate solution *between* the collocation points. The method is demonstrated on several examples of varying complexity and is found to be a viable method for efficiently and accurately solving complex optimal control problems using pseudospectral methods.

We note that hp-methods have been previously developed in the context of finite elements in mechanics and spectral methods in fluid dynamics. In particular, Refs. [20, 21, 22, 23, 24] describe the mathematical properties of h, p, and hp methods for finite elements. Ref. [25] showed the application of an hp-adaptive least-squares spectral element method (LS-SEM) for solving hyperbolic partial differential equations. Ref. [26] developed an adaptive spectral least-squares collocation scheme for the Burgers equation. Ref. [27] showed the use of an hp-adaptive LS-SEM for solving the population balance equation while Ref. [28] developed an hp-adaptive spectral element solver for reactor modeling. Finally, an overview of hp-adaptive spectral element methods for solving problems in computational fluid dynamics can be found in Ref. [29].

This paper is organized as follows. In Section 2 we provide a motivation for developing an hp-adaptive pseudospectral method. In Section 3 we present the formulation of a general Bolza optimal control problem. In Section 4 we describe the formulation of the Gauss pseudospectral method which is the basis for the implementation of the method presented in this paper. In Section 5 we describe the structure of the NLP that arises from global and segmented collocation. In Section 6 we present the hp-adaptive pseudospectral method. In Section 7 we provide several applications of the method to optimal control problems of varying complexity. In Sections 8 and 9 we provide a discussion of the results and some limitations of the method. Finally, in Section 10 we provide concluding remarks.

2 Motivation for an hp-Adaptive Pseudospectral Method

In order to motivate the development an hp-adaptive pseudospectral method, consider the following two functions:

$$y = \exp(\tau), \quad \tau \in [-1, 1] \tag{1}$$

$$y = \begin{cases} -1 & , \quad -1 \leq \tau \leq -1/2 \\ \tau & , \quad -1/2 \leq \tau \leq 1/2 \\ 1 & , \quad 1/2 \leq \tau \leq 1 \end{cases} \tag{2}$$

It is seen that Eq. (1) is smooth while Eq. (2) has a discontinuous first derivative at $\tau = \pm 1/2$.

Suppose that we approximate the function in Eq. (1) using a global approximation and a piecewise (segmented) approximation. The global approximation is obtained using a basis of Legendre polynomials, i.e.,

$$y(\tau) \approx Y(\tau) = \sum_{i=0}^{n} c_i \phi_i(\tau) \tag{3}$$

where for any given value of n the coefficients $c_i, \ (i = 0, \ldots, n)$ are determined in a least-squares sense. Fig. 1a shows the maximum error as a function of the polynomial degree, n. It is seen that the error decreases exponentially as a function n and is $\mathcal{O}(10^{-5})$ for $n = 5$. The piecewise approximation is obtained using evenly spaced intervals of constant functions such that each constant is the least-squares approximation in that interval. Fig. 1b shows the maximum error as a function of the *logarithm* of the number of intervals. Unlike the global approximation where the degree of the polynomial is increased, in this case it is seen that the error decreases extremely slowly as a function of the number of piecewise constant intervals. Thus, in this example convergence is achieved much more rapidly by increasing the degree of a global polynomial approximation as compared to using a piecewise fixed-degree polynomial and varying the number of intervals.

Suppose now that we use the global and piecewise approaches for approximating the function in Eq. (2) as we did to approximate the function in Eq. (1). Fig. 1c shows the maximum error as a function of the polynomial degree for the case where a global Legendre polynomial is used. Different from the results for the approximation of Eq. (1), in this case it is seen that the error decreases much more slowly as a function of polynomial degree. The slower convergence using a global polynomial is attributed to the fact that the function in Eq. (2) is not smooth, but is only piecewise smooth. Examining Fig. 1d, it is seen that, for any polynomial degree, the approximation error on the interior of the interval $\tau \in (-1, 1)$ is largest at the points where the derivative of the function is discontinuous (i.e., $\tau = \pm 1/2$). As expected, dividing the problem into segments at $\tau = \pm 1/2$, the function in Eq. (2) can be approximated exactly using a constant for $-1 \leq \tau \leq 1/2$, a straight line for $-1/2 \leq \tau \leq 1/2$, and a constant for $1/2 \leq \tau \leq 1$. Thus, it is seen for this second example that much more rapid convergence is achieved

by determining an appropriate segment decomposition and the degrees of the polynomials in each segment as compared with using a global polynomial approximation.

The preceding discussion demonstrates the key point that rapid convergence of an approximation to the true function depends upon the type of function that is being approximated. In the case of a smooth function, it is preferable to use a global approximation and determine the appropriate polynomial degree. In the case of a nonsmooth function it is preferable to divide the domain into subintervals, determine the locations of the segment breaks, and use a polynomial of "appropriate" degree in each subinterval. In general, it will be the case that convergence will be achieved most rapidly (as a function of polynomial degree) by using higher-degree polynomials in some segments while using lower-degree polynomials in other segments. With the aim of determining the appropriate segment decomposition (i.e., the locations and widths, h, of the segments) and the appropriate polynomial degree in each segment (i.e., the degree p in each segment), in this paper we develop a new hp-adaptive pseudospectral method for solving optimal control problems. In the context of optimal control, the break points between segments often correspond to those times where either control or state constraints change between active and inactive.

3 Optimal Control Problem in Bolza Form

Without loss of generality, consider the following optimal control problem in Bolza form. Minimize the cost functional

$$J = \mathbf{\Phi}(\mathbf{x}(-1), t_0, \mathbf{x}(+1), t_f) + \frac{t_f - t_0}{2} \int_{-1}^{1} \mathcal{L}(\mathbf{x}(\tau), \mathbf{u}(\tau), \tau)\, d\tau \tag{4}$$

subject to the dynamic constraints

$$\frac{d\mathbf{x}}{d\tau} = \frac{t_f - t_0}{2} \mathbf{f}(\mathbf{x}(\tau), \mathbf{u}(\tau), \tau), \tag{5}$$

the boundary conditions (i.e., the event constraints)

$$\boldsymbol{\phi}(\mathbf{x}(-1), t_0, \mathbf{x}(+1), t_f) = \mathbf{0}, \tag{6}$$

and the inequality path constraints

$$\mathbf{C}(\mathbf{x}(\tau), \mathbf{u}(\tau), \tau; t_0, t_f) \leq \mathbf{0}, \tag{7}$$

where $\mathbf{x}(\tau)$ is the state, $\mathbf{u}(\tau)$ is the control and τ is time. The variable $\tau \in [-1, 1]$ and $t \in [t_0, t_f]$ are related as

$$t = \frac{t_f - t_0}{2} \tau + \frac{t_f + t_0}{2} \tag{8}$$

4 State Approximation Using Pseudospectral Methods

A pseudospectral method is typically employed as a p-method where the state is approximated using a basis of global polynomials. In order to remain specific in this discussion, in this paper we choose the *Gauss pseudospectral method* [9, 10, 11, 30] as the foundation for developing our hp-adaptive method. We note, however, that the method developed in this paper can be adapted to other pseudospectral methods with only slight modifications. In the Gauss pseudospectral method, the state of the continuous Bolza problem is approximated as

$$\mathbf{x}(\tau) \approx \mathbf{X}(\tau) = \sum_{i=0}^{N} \mathbf{X}_i L_i(\tau) \tag{9}$$

where $\tau \in [-1, 1]$, $L_j(\tau),\ (j = 0, \ldots, N)$ is a basis of Lagrange polynomials,

$$L_i(\tau) = \prod_{\substack{j=0 \\ j \neq i}}^{N} \frac{\tau - \tau_j}{\tau_i - \tau_j}, \quad (i = 0, \ldots, N), \tag{10}$$

and $\mathbf{X}_i \equiv \mathbf{X}(\tau_i),\ (i = 0, \ldots, N)$ are *row vectors* corresponding to the approximation of the state at the interpolation points $(\tau_0, \ldots, \tau_N)$, i.e.,

$$\mathbf{X}_i = \left[\begin{array}{ccc} X_{i1} & \cdots & X_{in} \end{array} \right], \quad (i = 0, \ldots, N),$$

where we recall that n is the dimension of the state. The interpolation points in the Gauss pseudospectral method are the initial point $\tau_0 = -1$ and the N Legendre-Gauss [31] (LG) points $(\tau_1, \ldots, \tau_N)$, where the LG points lie strictly on the interior of the interval $[-1, 1]$ and are the roots of the N^{th}-degree Legendre polynomial [32], $P_N(\tau)$. It is known that the Lagrange polynomials satisfy the property

$$L_i(\tau_j) = \delta_{ij}, \quad (i = 0, \ldots, N),\ (j = 1, \ldots, N) \tag{11}$$

where δ_{ij} is the Kronecker Delta function. Differentiating Eq. (9), we obtain

$$\dot{\mathbf{x}}(\tau) \approx \dot{\mathbf{X}}(\tau) = \sum_{i=0}^{N} \mathbf{X}(\tau_i) \dot{L}_i(\tau). \tag{12}$$

The derivative of the state approximation given in Eq. (12) is then collocated at the N Legendre-Gauss points. Treating the m-dimensional control at each LG point as a row vector,

$$\mathbf{U}_i = \left[\begin{array}{ccc} U_{i1} & \cdots & U_{im} \end{array} \right], \quad (i = 1, \ldots, N),$$

the continuous-time dynamics of Eq. (5) lead to the collocation conditions:

$$\mathbf{D}\mathbf{X} - \frac{t_f - t_0}{2} \mathbf{F} = \mathbf{0}, \tag{13}$$

where $\mathbf{D} \in \mathbb{R}^{N\times(N+1)}$ is the Gauss pseudospectral differentiation matrix [9, 10, 11, 12] and

$$\begin{gathered}\mathbf{X} = \begin{bmatrix} \mathbf{X}_0 \\ \vdots \\ \mathbf{X}_N \end{bmatrix} \quad , \quad \mathbf{X}^{\mathsf{LG}} = \begin{bmatrix} \mathbf{X}_1 \\ \vdots \\ \mathbf{X}_N \end{bmatrix} \quad , \quad \mathbf{U}^{\mathsf{LG}} = \begin{bmatrix} \mathbf{U}_1 \\ \vdots \\ \mathbf{U}_N \end{bmatrix} \quad , \quad \boldsymbol{\tau}^{\mathsf{LG}} = \begin{bmatrix} \tau_1 \\ \vdots \\ \tau_N \end{bmatrix} \quad , \\ \mathbf{F} = \mathbf{F}(\mathbf{X}^{\mathsf{LG}}, \mathbf{U}^{\mathsf{LG}}, \boldsymbol{\tau}^{\mathsf{LG}}; t_0, t_f) = \begin{bmatrix} \mathbf{f}(\mathbf{X}_1, \mathbf{U}_1, \tau_1; t_0, t_f) \\ \vdots \\ \mathbf{f}(\mathbf{X}_N, \mathbf{U}_N, \tau_N; t_0, t_f) \end{bmatrix}.\end{gathered} \tag{14}$$

In addition, an NLP variable corresponding to the state at the terminal point, $\mathbf{X}_{N+1} = \mathbf{X}(\tau_{N+1}) = \mathbf{X}(+1)$, is included by adding the following Legendre-Gauss quadrature approximation to the integral of the dynamics at $\tau = +1$:

$$\mathbf{X}_{N+1} = \mathbf{X}_0 + \frac{t_f - t_0}{2}\mathbf{w}^{\mathsf{T}}\mathbf{F} \tag{15}$$

where $\mathbf{w}$ is a column vector of the Legendre-Gauss weights [31]. Next, the cost functional of Eq. (4) is approximated using a Legendre-Gauss quadrature as

$$J \approx \Phi(\mathbf{X}_0, t_0, \mathbf{X}_{N+1}, t_f) + \frac{t_f - t_0}{2}\sum_{i=1}^{N} w_i \mathcal{L}[\mathbf{X}_i, \mathbf{U}_i, \tau_i; t_0, t_f] \tag{16}$$

The system of algebraic equations corresponding to the dynamics resulting from the Gauss pseudospectral discretization are then given as

$$\mathbf{D}\mathbf{X} - \frac{t_f - t_0}{2}\mathbf{F} = \mathbf{0} \tag{17}$$

$$\mathbf{X}_{N+1} - \mathbf{X}_0 - \frac{t_f - t_0}{2}\mathbf{w}^{\mathsf{T}}\mathbf{F} = \mathbf{0} \tag{18}$$

Finally, the boundary conditions and path constraints of Eqs. (6) and (7) are given, respectively, as

$$\boldsymbol{\phi}(\mathbf{X}_0, t_0, \mathbf{X}_{N+1}, t_f) = \mathbf{0} \tag{19}$$

$$\mathbf{C}(\mathbf{X}_i, \mathbf{U}_i, \tau_i; t_0, t_f) \leq \mathbf{0}, \quad (i = 1, \ldots, N). \tag{20}$$

The NLP arising from the GPM is then to minimize the cost function of (16) subject to the algebraic constraints of Eqs. (17)–(20).

While the aforementioned approach for approximation, differentiation, and collocation is common to most pseudospectral methods, a key assumption when using a pseudospectral method is that a solution to the NLP is a good approximation to the solution of the optimal control problem. This assumption is only valid if the approximating global polynomial is of sufficiently large degree. If, however, the approximating polynomial is of too small a degree, the left-hand side of Eq. (17), when $\mathbf{X}$ is replaced by the interpolant of the exact solution, may not be very small. In addition, using a

sufficiently large-degree polynomial approximation will result not only in an accurate solution *at* the support points, but it will also result in an accurate solution *between* the support points (that is, the Lagrange interpolating polynomial will produce an accurate approximation at an arbitrary point in the domain). Using a global polynomial, the common practice is to increase the number of support points until the required accuracy is obtained. Many applications exist, however, where an accurate solution can only be obtained using a very large-degree global polynomial. If the degree of the polynomial is too large, the resulting NLP from a pseudospectral discretization may be computationally intractable.

In this paper, an hp-adaptive pseudospectral method is developed. The objective of the method is to determine the number of spectrally collocated segments and the degree of the polynomial in each segment that provides an accurate approximation to the solution of the Bolza optimal control problem defined in Section 3. As we will demonstrate, the approach developed provides an accurate approximation of the state at the collocation points and *between* the collocation points [via evaluation of the Lagrange polynomial approximation of Eq. (9)]. In addition, the method presented in this paper is more computationally efficient than using purely global collocation. The basis of the method is a two-tiered strategy that determines the number and locations of the segments and the degree of the polynomial approximation required in each segment.

5 Multiple-Segment NLP Using a Pseudospectral Method

A detailed description of the NLP resulting from a global pseudospectral discretization has been described in Ref. [13]. A brief discussion and the extension of pseudospectral methods to multiple-segment problems is described in this section. As described in Ref. [13], the NLP decision variables for a global pseudospectral discretization include those corresponding to the state, control, initial time, and terminal time. Denoting these partitions of the vector of decision variables by $\mathbf{z}_x$, $\mathbf{z}_u$, t_0, and t_f, respectively, the complete vector of decision variables is given as

$$\mathbf{z} = \begin{bmatrix} \mathbf{z}_x \\ \mathbf{z}_u \\ t_0 \\ t_f \end{bmatrix}. \tag{21}$$

Collocating the dynamics for each scalar differential equation gives rise to a constraint Jacobian whose main-diagonal block is a full matrix of size $\approx N \times N$, where N is the number of global collocation points. Qualitatively, the sparsity pattern of the constraint Jacobian resulting from global collocation has the form shown in Fig. 2a, where the $\approx N \times N$ blocks are seen on the main diagonal of the sparsity

pattern. It is seen that as the majority of nonzero elements in the sparsity pattern are those due to the $\approx N^2$ elements in the diagonal blocks.

Suppose now that we use N collocation points, but divide the problem into S segments such that

$$N = \sum_{s=1}^{S} N_s \tag{22}$$

where N_s is the number of collocation points within each segment and N is an equivalent number of global collocation points. Eq. 13 and 15 are then applied across each segment. Therefore, the system of algebraic equations corresponding to the dynamics from the segmented Gauss pseudospectral discretization are then given in matrix form as

$$\begin{bmatrix} \mathbf{D}_1 & \mathbf{0} & \cdots & \mathbf{0} \\ \mathbf{0} & \mathbf{D}_2 & \cdots & \mathbf{0} \\ \vdots & & \ddots & \vdots \\ \mathbf{0} & \cdots & \mathbf{0} & \mathbf{D}_S \end{bmatrix} \mathbf{X} = \begin{bmatrix} \frac{t_1-t_0}{2}\mathbf{I}_1 & \mathbf{0} & \cdots & \mathbf{0} \\ \mathbf{0} & \frac{t_2-t_1}{2}\mathbf{I}_2 & \cdots & \mathbf{0} \\ \vdots & & \ddots & \vdots \\ \mathbf{0} & \cdots & \mathbf{0} & \frac{t_S-t_{S-1}}{2}\mathbf{I}_S \end{bmatrix} \mathbf{F} \tag{23}$$

where t_s denotes the end of the s^{th} segment and $\mathbf{I}_s,\ (s = 1, \ldots, S)$ are identity matrices of appropriate size. From the Gauss pseudospectral method [9, 10, 11, 30], the state at the terminus of each segment is approximated using a Legendre-Gauss quadrature,

$$\mathbf{X}^s_{N_s+1} \quad = \quad \mathbf{X}^s_0 + \tfrac{t_s-t_{s-1}}{2} \textstyle\sum_{i=1}^{N_s} w^s_i \mathbf{f}^s_i \quad , \quad (s = 1, \ldots, S) \tag{24}$$

where w^s_i and $\mathbf{f}^i_s$ $(i = 1, \ldots, N_s)$ are, respectively, the Legendre-Gauss quadrature weights and the right hand side of the dynamic equations evaluated at each of the N_s collocation points in segment s. Continuity on the state at a segment interface is maintained by using the same NLP variable for the value of the state at the end of segment s and the beginning of segment $s + 1$.

Qualitatively, the segmented sparsity pattern is shown in Fig. 2b. It is seen that the segmented sparsity pattern has significantly fewer nonzero elements than an equivalently sized globally collocated problem due to the fact that each diagonal block is much smaller and has many fewer nonzeros when compared to equivalently sized globally collocated diagonal block. An example of how the density of the Jacobian decreases is as follows. For a six state, two control, and one path constraint problem using 30 global collocation points, the NLP has 255 decision variables and is 14 percent dense. An equivalent NLP that employs three segments with 10 collocation points in each segment has 267 decision variables and is 7 percent dense.

It is seen from the preceding description that dividing a problem into segments results in a much sparser NLP when compared with global collocation. It is noted, however, that a trade-off exists between segmented and global collocation. Using low-degree polynomials may require a very large

number of segments in order to obtain a given accuracy. In addition, spectral accuracy (a key property of a pseudospectral method) is lost as the degree of the polynomial is decreased within a segment. On the other hand, using larger-degree polynomials may lead to the same accuracy with many fewer segments, but may result on a computationally expensive NLP. In order to retain as close to spectral accuracy as possible without excessive computational burden, the method developed in this paper utilizes a segmented approach that detects when spectral accuracy may be lost (e.g., detection of non-smoothness in the solution, stiff problems with large time-scale discrepancies). As a result, the method of this paper will result in fewer optimization variables as compared with a strictly global method. In addition, the method provides refinement in regions where it may be necessary. Consequently, the sparsity of the NLP using the method of this paper is much greater than would be obtained with a purely global pseudospectral method.

6 hp-Adaptive Pseudospectral Method

Suppose that the trajectory on the time interval $t \in [t_0, t_f]$ has already been divided into S segments such that the time span of segment $s \in [1, \ldots, S]$ is $[t_{s-1}, t_s]$ and N_s is the number of collocation points allocated in each segment. The objective of the hp-adaptive pseudospectral is to determine if a segment should either be divided into more segments and the locations of the newly created segments, or if the number of collocation points in a segment should be increased.

6.1 Criteria for Determining if a Segment Should Be Divided

The criteria for segment division or collocation point increase is based on how closely the dynamic constraints are satisfied at the midpoints of the collocation points, $(\bar{t}_1, \ldots, \bar{t}_N) \in [t_{s-1}, t_s]$, i.e.,

$$\bar{t}_i = \frac{t_i + t_{i+1}}{2}, \quad (i = 1, \ldots, N_s - 1) \tag{25}$$

Correspondingly, let $\bar{\mathbf{X}}$ and $\bar{\mathbf{U}}$ be $(N_s - 1) \times n$ and $(N_s - 1) \times m$ matrices (where n is the number of states and m is the number of controls),

$$\bar{\mathbf{X}} = \begin{bmatrix} \mathbf{X}(\bar{t}_1) \\ \vdots \\ \mathbf{X}(\bar{t}_{N_s-1}) \end{bmatrix} \quad , \quad \bar{\mathbf{U}} = \begin{bmatrix} \mathbf{u}(\bar{t}_1) \\ \vdots \\ \mathbf{u}(\bar{t}_{N_s-1}) \end{bmatrix} \tag{26}$$

where the i^{th} row of $\bar{\mathbf{X}}$ and $\bar{\mathbf{U}}$ corresponds to the approximation of the state or control in segment s at the i^{th} midpoint between two collocation points, $\bar{t}_i$. The midpoint approximations of the state are obtained using the Lagrange polynomial approximation of Eq. (9) while the midpoint approximations for the control are obtained using the arbitrary choice of cubic interpolation. Next, let $\bar{\mathbf{D}}$ be a square

$(N_s-1)\times(N_s-1)$ differentiation matrix computed using the hp-adaptive pseudospectral method of Ref. [33] with the values $\boldsymbol{\tau}=(\bar{\tau}_1,\ldots,\bar{\tau}_{N_s-1})\in[-1,1]$, where $(\bar{\tau}_1,\ldots,\bar{\tau}_{N_s-1})$ are computed using Eq. (8). Finally, let $\mathbf{R}$ be the $(N_s-1)\times n$ matrix

$$\mathbf{R}=\left|\bar{\mathbf{D}}\bar{\mathbf{X}}-\frac{t_s-t_{s-1}}{2}\mathbf{F}(\bar{\mathbf{X}},\bar{\mathbf{U}},\boldsymbol{\tau};\mathbf{p},t_{s-1},t_s)\right|\in\mathbb{R}^{(N_s-1)\times n} \tag{27}$$

where $|\cdot|$ denotes the absolute value of each element of the matrix $\mathbf{R}$. The elements of the matrix $\mathbf{R}$ will be referred to as the *midpoint residuals* of the dynamics at the midpoints of the collocation points and the matrix $\mathbf{R}$ itself will be referred to as the *midpoint residual matrix*. Each column of the matrix $\mathbf{R}$ provides a measure of the amount by which the state violates the collocation equations at the midpoints between two collocation points in segment s.

Suppose we let $\mathbf{r}$ be the elements of the column of the midpoint residual matrix $\mathbf{R}$ that contains the largest element of $\mathbf{R}$. Then $\mathbf{r}$ can be written in component form as

$$\mathbf{r}=\begin{bmatrix} r(\bar{t}_1)\\ \vdots\\ r(\bar{t}_{N_s-1})\end{bmatrix} \tag{28}$$

where each component, $r(\bar{t}_i),\ (i=1\ldots,N_s-1)$ of $\mathbf{r}$ corresponds to the element of $\mathbf{r}$ at the midpoint time $\bar{t}_i,\ (i=1,\ldots,N_s-1)$. Because $\mathbf{r}$ contains the maximum element in the matrix $\mathbf{R}$, it is used as the metric to determine if the segment should be further subdivided and, if so, where the segment breaks should be placed, or if the number of collocation points in the segment should be increased.

Suppose now that we let $\bar{r}$ be the arithmetic mean of the components of the vector $\mathbf{r}$, that is

$$\bar{r}=\frac{\sum_{i=1}^{N_s-1}r(\bar{t}_i)}{N_s-1} \tag{29}$$

Next, define

$$\boldsymbol{\beta}=\begin{bmatrix}\beta(\bar{t}_1)\\ \vdots\\ \beta(\bar{t}_1)\end{bmatrix}=\begin{bmatrix} r(\bar{t}_1)/\bar{r}\\ \vdots\\ r(\bar{t}_{N_s-1})/\bar{r}\end{bmatrix} \tag{30}$$

The vector $\boldsymbol{\beta}$ will be referred to as the *scaled midpoint residual vector*. Each element of the vector $\boldsymbol{\beta}$ is a scaled measure of the amount by which the collocation conditions at a particular midpoint differs from zero.

6.2 Behavior of Scaled Midpoint Residual Vector

The scaled midpoint residual vector $\boldsymbol{\beta}$ can have two behaviors that are relevant in the method of this paper. The first possibility is that all of the components of $\boldsymbol{\beta}$ are approximately the same size.

For these "uniform-type" errors in the collocation conditions at $(\bar{t}_1, \ldots, \bar{t}_{N_s-1})$ the hp-method is designed to increase the number of collocation points in the segment. The second possibility is that certain components of $\boldsymbol{\beta}$ are significantly larger than other components of $\boldsymbol{\beta}$ in the segment. For this "non-uniform-type" error, the method is designed to place a segment break at the locations of these large violations in the collocation equations. The vector $\boldsymbol{\beta}$ is used to determine the locations of new segments or if the number of collocation points in a segment are increased.

6.3 Determining Locations of New Segments or Increase in Number of Collocation Points

Let ϵ be a user-defined tolerance and **assume that the maximum entry of Eq. (27) is greater than** ϵ. In this case, the segment either needs to be divided into more segments or the degree of the polynomial approximation needs to be increased in order to reach the tolerance ϵ. In order to improve the accuracy of Eq. (27), we use the following strategy. Let ρ be a user-specified threshold for the size of the elements of the vector $\boldsymbol{\beta}$. Again assuming that Eq. (27) exceeds the tolerance ϵ, two types of errors are relevant in the method of this paper: (1) isolated elements of $\boldsymbol{\beta}$ are greater than ρ, resulting in "non-uniform-type errors" and (2) no elements of $\boldsymbol{\beta}$ exceed ρ, resulting in "uniform-type-errors." For the case of non-uniform-type errors, the segment is divided while for uniform-type-errors the number of collocation points in the segment is increased. We now explain how segments are divided and collocation points are increased.

Segment Division for Non-Uniform-Type Errors: For non-uniform-type errors, the segment is divided at the time points where the entries of vector $\boldsymbol{\beta}$ are greater than ρ. Often, Eq. (30) contains adjacent entries which are greater than ρ. In such cases, the segment is divided at only the locations of the largest element of $\boldsymbol{\beta}$ that exceeds ρ. Fig. 3 provides a schematic of how a segment is divided into more segments for the case where elements of $\mathbf{R}$ in Eq. (27) exceed ϵ.

Collocation Point Increase for Uniform-Type Errors: For uniform-type errors, suppose further that every element of the vector $\boldsymbol{\beta}$ is less than ρ. In this case the violations in the dynamic collocation equations at the midpoints of the collocation points are of "uniform-type." In this case the number of collocation points in the segment is increased by a user-specified amount L, that is

$$N_s^{(k+1)} = N_s^{(k)} + L \tag{31}$$

where $N_s^{(k)}$ is the number of collocation points in segment s on grid iteration k. Once the maximum entry of Eq. (27) is less than ϵ, the segment is neither divided further nor is the number of collocation points increased.

6.4 Stopping Criteria

The iterative procedure terminates when the dynamic constraints, the path constraints, and the bounds on the state and control are satisfied to within the specified tolerance ϵ in all segments when evaluated at the midpoints of the collocation points. For the dynamic constraints, the stopping criteria imposes that every entry of $\mathbf{R}$ in Eq. (27) lie below ϵ. In the case of the path constraints or bounds on the state and control, the stopping criteria imposes that all violations in constraints or bounds be less than ϵ. In the case that the dynamic constraints are satisfied but either the path constraints or the bounds on the state and control are not, then modification of the segments continues as in Section 6.3 until both the path constraints or the bound constraints are satisfied to the tolerance ϵ.

6.5 Qualitative Notions of User-Defined Parameters ρ and ϵ

User-Defined Parameter ρ***:*** The parameter ρ represents a tuning parameter that weights the method between a local and global strategy. For large values of ρ, the method employs global collocation because none of the entries of $\boldsymbol{\beta}$ will be large enough to require that a segment be divided. As ρ is decreased, the method becomes a local because a greater number of points in the segment will be such that the elements in $\boldsymbol{\beta}$ are greater than ρ (thus resulting in the problem being divided into more segments). It is noted that ρ should always be greater than one because values of $\rho \leq 1$ will always result in a segment break.

User-Defined Tolerance ϵ***:*** The tolerance ϵ provides a threshold for the accuracy of the dynamic constraints and path constraints of the continuous-time optimal control problem. Specifically, the smaller the value of ϵ, the greater the required accuracy is in the dynamics. In addition, due to the stopping criteria, the parameter ϵ provides a threshold for the required accuracy of the state approximation. In this study we assume that ϵ is less than unity where the NLP is itself scaled such that the variables and constraints are $\mathcal{O}(1)$. In the case of a poorly scaled NLP, the pseudospectrally discretized problem may not be solvable, thus resulting in ϵ being meaningless because the hp-adaptive method cannot be implemented in this case.

6.6 Iterative Procedure for hp-Adaptive Pseudospectral Method

The following iterative procedure summarizes the aforementioned approach to collocation point increase and segment division:

(i) Initialize the problem choosing M collocation points, where M is chosen by the user.

(ii) Solve the NLP with the prescribed grid distribution.

(iii) Check for each segment if the dynamic constraints, path constraints, and bounds on the state and control are satisfied to the tolerance ϵ in each segment at the midpoints between collocation points. For all segments not within the prescribed tolerance, continue to step (iv) or step (v).

(iv) For all segments where Eq. (30) is of "uniform-type" increase the number of collocation points in these segments by the user-specified amount L.

(v) For all segments where Eq. (30) is of "non-uniform-type," break the segments at all prescribed points (see Fig. 3) and set $M = 5$ in each new segment.

(vi) After all segments have been updated, return to step (ii).

(vii) Terminate when the dynamic constraints, path constraints, and bounds on the state and control are satisfied to the tolerance ϵ in all segments.

6.7 Clarification of Various Aspects of hp-Adaptive Pseudospectral Method

Several important aspects of the hp-adaptive pseudospectral method are now clarified. We choose $L = 10$ for this paper because increasing by fewer than ten collocation points may result in a significantly larger number of grid iterations. Whenever the method adds a segment, the number of collocation points in the newly created segment is set to five in order to keep the number of collocation points small. The error estimate of Eq. (27) has been found in practice to result in an appropriate termination of the method and to keep the NLP of reasonable size. To avoid the case where large, computationally inefficient polynomial approximations are being used to approximate a segment, a user specified limit on the number of collocation points within a segment should be set. If this limit is exceeded, then the current segment should be subdivided to avoid computationally large, dense segments. For the problems of this paper, this scenario was not encountered.

7 Examples

We now apply the hp-adaptive pseudospectral method of Section 6 to several examples. All of the examples analyzed in this section are taken from the open literature and were solved using a modified version of the open-source pseudospectral optimal control software GPOPS [12, 13][†] using the NLP solver SNOPT [34]. All computations were performed on a 2 GHz Core 2 Duo machine with 2 gigabytes of RAM running OpenSuse Linux 11.0 and MATLAB R2007a.

[†]GPOPS[12, 13] is available for download at either http://www.sourceforge.net/projects/gpops or http://www.gpops.org.

In the results that follow, the state approximation is shown at the discretization points (collocation points plus endpoints) and at points between the discretization points. The state approximation at points between the discretization points was obtained using the Lagrange polynomial approximation of Eq. (9) on a very fine grid in each segment. On the other hand, the control is shown at only the collocation points because it does not have a unique function approximation between the collocation points. Finally, Example 1 has an analytic solution while Examples 2 through 5 do not have an analytic solution. Thus, for Example 1 the actual error in the solution on the final grid will be computed. For Examples 2 through 5, the error on the final grid will be estimated by solving the NLP using one additional collocation point, $N_s + 1, \in [1, \ldots, S]$, in each segment and taking the difference between the N_s and $N_s + 1$ state approximations.

Example 1: Moon-Lander Problem

Consider the following optimal control problem of a soft lunar landing [35]. Minimize

$$J = \int_{t_0}^{t_f} u dt \tag{32}$$

subject to

$$\begin{aligned} \dot{h} &= v \\ \dot{v} &= -g + u, \end{aligned} \tag{33}$$

the boundary conditions

$$\begin{aligned} h(0) &= 10 \quad , \quad v(0) = -2 \\ h(t_f) &= 0 \quad , \quad v(t_f) = 0, \end{aligned} \tag{34}$$

and the control path constraint

$$0 \leq u \leq 3 \tag{35}$$

where $g = 1.5$, and t_f is free. The optimal solution to the optimal control problem given in Eqs. (32)–(35) is given as

$$(h^*(t), v^*(t), u^*(t)) = \begin{cases} (-\frac{3}{4}t^2 + v_0 t + h_0, -\frac{3}{2}t + v_0, 0) & , \quad t \leq s^* \\ (\frac{3}{4}t^2 + (-3s^* + v_0)t + \frac{3}{2}(s^*)^2 + h_0, \frac{3}{2}t + (-3s^* + v_0), 3) & , \quad t \geq s^* \end{cases} \tag{36}$$

where s^* is given as

$$s^* = \frac{t_f^*}{2} + \frac{v_0}{3} \tag{37}$$

with

$$t_f^* = \frac{2}{3}v_0 + \frac{4}{3}\sqrt{\frac{1}{2}v_0^2 + \frac{3}{2}h_0} \tag{38}$$

For the boundary conditions given in Eq. (34), we have $(s^*, t_f^*) = (1.4154, 4.1641)$. It is seen that the optimal control for this problem is "bang-bang" in that it is at its minimum value for $t < s^*$ and at its maximum value for $t > s^*$.

Fig. 4a shows the control for this problem for $\epsilon = 10^{-3}$ while Fig. 4b shows the distribution of collocation points on each iteration of the method. Initializing the problem with five global collocation points, it is seen that the method progresses to a final grid such that the collocation points are more densely located near the control discontinuity, terminating with a six-segment decomposition of five collocation points in each segment except the segment containing the discontinuity terminated with 15 collocation points. Segment breaks occurred at $t = (1.30, 1.37, 1.41, 1.45, 1.70)$. Furthermore, the control discontinuity is closely bracketed by a fairly short segment. Fig. 4c displays the state for this problem, and demonstrates that the nonsmoothness in the state at s^* is accurately captured. Table 1 shows the performance of the method using $\rho = 3$ in comparison with a global approach. It is seen that, when a highly accurate solution is desired, the global approach is simultaneously more computationally expensive and less accurate than the hp-adaptive method. For example, Table 1 shows that a solution using 200 global collocation points achieves a maximum state error of $\mathcal{O}(10^{-3})$ while a solution obtained using the hp-adaptive method with 45 collocation points achieves a maximum state error of $\mathcal{O}(10^{-6})$. In the case of global collocation with $\epsilon = 10^{-1}$, a solution was never obtained because the maximum value in Eq. (27) only reduced to $\mathcal{O}(1)$, even for 200 global collocation points. On the other hand, the hp-adaptive method was able to solve this problem much more computationally efficiently and for a much smaller value of $\epsilon = 10^{-4}$. Examining the maximum of Eq. (27) and the maximum relative error between the NLP solution and the true solution, for this problem, it is seen that analyzing the value of dynamic collocation at the midpoints between collocation points is a conservative estimate of the actual errors in the state (the actual state errors being an order of magnitude or two smaller than ϵ).

Example 2: Hyper-Sensitive Problem

Consider the following *hyper-sensitive* [36, 37, 38, 39] optimal control problem adapted from Ref. [37]. Minimize the cost functional

$$J = \frac{1}{2}\int_0^{t_f} (x^2 + u^2)dt \tag{39}$$

subject to the dynamic constraint

$$\dot{x} = -x^3 + u \tag{40}$$

and the boundary conditions

$$x(0) = 1 \quad , \quad x(t_f) = 1 \tag{41}$$

where t_f is fixed. It is known that for sufficiently large values of t_f that the solution to this example exhibits a so called "take-off", "cruise", and "landing" structure where the interesting behavior occurs near the initial and final time (see Ref. [37] for details). In particular, the "cruise" segment of this trajectory is constant (i.e., state, control and, interestingly, costate are all zero) and becomes an increasingly large percentage of the total trajectory time as t_f increases. Given the structure of the solution, one would expect that the majority of collocation points would be placed in the "take-off" and "landing" segments while few collocation points would be placed in the "cruise" segment.

Suppose we use a global polynomial to approximate the solution. Fig. 5a shows the solution for $t_f = 40$ using three different approximations. It is seen that an insufficient degree polynomial (5 and 10 collocation points) results in an inaccurate solution (the solution is inaccurate in the "take off" and "landing" segments and also oscillates around the true solution in the "cruise" segment). It should be noted that not only are the interpolation points between the discretization points inaccurate, but the discretization points themselves can be highly inaccurate when utilizing an insufficient degree global polynomial. On the other hand, utilizing a 25^{th}-degree polynomial (i.e., 25 collocation points) results in a solution that is in better agreement with the optimal solution. It is expected that, as t_f increases, the degree of a *global* polynomial required to solve the problem will also increase.

This example was solved using the hp-adaptive pseudospectral method of Section 6 for different values of t_f using global collocation and an initial grid of five global collocation points. It is seen from Table 2 that the problem only solved for relatively large values of ϵ; for smaller values of ϵ, the problem did not solve. Even for loose tolerances, for large final times, a global polynomial did not accurately approximate the solution. Also, utilizing such a large number of global collocation points will become computationally intractable for higher-dimensional problems (i.e., problems with many more states and controls) due to the increased memory and computational requirements associated with such a dense NLP.

Suppose now that the hp-adaptive pseudospectral method is applied to this example using $\rho = 3$ (thus, forcing the method to divide the problem into segments) and $\epsilon = 10^{-3}$, where $\epsilon = 10^{-3}$ was chosen because this value results in very accurate solutions while maintaining a small computation time. The results obtained using $\rho = 3$ and $\epsilon = 10^{-3}$ are shown in Table 3. It is seen that for large values of t_f the number of collocation points are increased, but the problem is still manageable in terms of CPU time, NLP variables and Jacobian entries. Figs. 5b, 5c, and 5d show the solution for $t_f = 5000$ along with the solution obtained using $\mathbb{SOCS}$ [40]. The hp-adaptive pseudospectral solutions and $\mathbb{SOCS}$ solutions are in excellent agreement. As one might expect, the majority of collocation points are placed in the take-off and landing segments, while many fewer collocation points are placed in the cruise segment. With regard to CPU time, it is seen that the total computation time using $\rho = 3$ is

growing as t_f grows but not by a significant amount. Because the problem is divided into segments, the resulting NLP is significantly more sparse as compared with using global collocation. Also, unlike global collocation, where no solution was obtained for $t_f > 200$, using $\rho = 3$ we were able to obtain solutions for $t_f = 5000$. The final grid for $t_f = 5000$ was increased by one collocation point in each segment, the NLP was re-solved, and the maximum difference between the state approximations between these two grids was $\mathcal{O}(10^{-4})$.

Example 3: Dynamic Soaring Problem

Consider the following optimal control problem taken from Ref. [41]. Minimize

$$J = \beta \tag{42}$$

subject to the dynamic constraints

$$\begin{array}{rclcrcl}
\dot{x} & = & V\cos\gamma\sin\Psi + W_x & , & m\dot{V} & = & -D - mg\sin\gamma - m\dot{W}_x\cos\gamma\sin\Psi \\
\dot{y} & = & V\cos\gamma\cos\Psi & , & mV\dot{\gamma} & = & L\cos\sigma - mg\cos\gamma + m\dot{W}_x\sin\gamma\sin\Psi \\
\dot{h} & = & V\sin\gamma & , & mV\cos\gamma\dot{\Psi} & = & L\sin\sigma - m\dot{W}_x\cos\Psi
\end{array} \tag{43}$$

and the boundary conditions

$$\begin{array}{rcl}
(x(0), y(0), h(0)) & = & (0, 0, 0) \\
(x(t_f), y(t_f), h(t_f)) & = & (0, 0, 0),
\end{array} \tag{44}$$

where β is the average wind gradient slope, W_x is the wind component along the East direction, m is the glider mass, V is the air-relative speed, Ψ is the heading angle measured clockwise from the North, γ is the air-relative flight path angle, h is the altitude, (x, y) are (East, North) position, σ is the glider bank angle, D is the drag force, and L is the lift force. The drag and lift forces are computed as

$$\begin{array}{rcl}
D = & qSC_D \\
L = & qSC_L
\end{array} \tag{45}$$

where $q = \rho V^2/2$ is the dynamic pressure, S is the vehicle reference area, $C_D = C_{D0} + KC_L^2$ is the coefficient of drag, and C_L is the coefficient of lift (where $0 \leq C_L \leq C_{L,\max}$). For this example, $C_{D0} = 0.00873$, $K = 0.045$, and $C_{L,\max} = 1.5$. Finally, it is noted that C_L and σ are the controls.

This example was posed in English units, but was solved using the automatic scaling procedure in GPOPS (see Ref. [30] for details). The hp-adaptive pseudospectral solution with $\rho = 3$ and $\epsilon = 10^{-3}$ and an initial grid of 10 global collocation points is shown in Figs. 6a–6e, while the Hamiltonian is shown in Fig. 6f. It is seen that the Hamiltonian is close to zero for this problem, consistent with the known optimal value. Table 4 summarizes the computational performance of both the global

pseudospectral method and the hp-adaptive pseudospectral method using $\rho = 3$. It is seen that the NLP was solvable using global collocation only for $\epsilon > 5 \times 10^{-2}$. In addition, for a similar value of ϵ, fewer collocation points were utilized with the hp-method as compared with global collocation. For this example similar computational effort was required using either a global method or the hp-method. Finally, for $\epsilon = (10^{-1}, 10^{-2}, 10^{-3})$, the maximum relative differences in the state on the final grid and the solution obtained from the NLP via a one collocation point increase in each segment were $(\mathcal{O}(10^{-2}), \mathcal{O}(10^{-3}), \mathcal{O}(10^{-3}))$.

Example 4: Minimum Time-to-Climb of a Supersonic Aircraft

Consider the following optimal control problem which is a variation of the *minimum time-to-climb of a supersonic aircraft* [42, 43, 38]. Minimize the cost functional

$$J = t_f \tag{46}$$

subject to the dynamic constraints

$$\dot{h} = v \sin\gamma, \quad , \quad \dot{E} = \frac{v}{W}(T - D), \quad , \quad \dot{\gamma} = \frac{g}{v}(n - \cos\gamma), \tag{47}$$

the boundary conditions

$$\begin{array}{rclcrcl} h(0) & = & 0 & , & h(t_f) & = & 19995 \text{ m} \\ E(0) & = & 852.6 \text{ m} & , & E(t_f) & = & 24435 \text{ m} \\ \gamma(0) & = & 0 \text{ deg} & , & \gamma(t_f) & = & 0 \text{ deg}, \end{array} \tag{48}$$

and the inequality path constraint

$$\gamma \leq 45 \text{ deg}, \tag{49}$$

where h is the altitude, E is the energy altitude, γ is the flight path angle, $v = \sqrt{2g(E-h)}$ is the speed, g is the local acceleration due to gravity, and n is the load factor (and is the control for this example). Further details of the vehicle model and the numerical values of the constants for this model can be found in Ref. [43] and [38].

The solution to the optimal control problem of Eqs. (46)–(48) using the hp-adaptive pseudospectral method is shown in Figs. 7 for $\epsilon = 10^{-3}$ and $\rho = 3$. A key characteristic of the performance of the hp-method is captured in Fig. 7a, where the flight path angle, γ, is shown to reach the path constraint. The path constraint is active from approximately $t = 18.45$ s to $t = 31.42$ s, after which γ decreases to near zero at $t \approx 100$ s. On its second increase, γ does not attain its maximum allowable value. Because the first increase hits the upper limit on γ (in this case, $\gamma_{\max} = 45$ deg), many collocation points and segments are required in order to obtain an accurate approximation. Also, the Hamiltonian, H, is

shown in Fig. 7e where it is seen that H is close to -1, (where the optimal Hamiltonian, H^* is -1 for this problem). Table 5 displays the computation times and expense for this example using various values of ϵ. Again, for even a very loose accuracy tolerance, the global approximation never converged while a segmented approach converged for increasingly tight tolerances. In this problem it is seen that obtaining an accurate solution to accuracy $\mathcal{O}(10^{-4})$ requires significantly more collocation points, segments, and CPU time. For $\epsilon = (10^{-1}, 10^{-2}, 10^{-3})$, the maximum relative difference between the state approximation on the final grid and grid with one extra collocation point per segment was approximately one order of magnitude less than ϵ. For $\epsilon = 10^{-4}$, this same maximum relative difference was $\mathcal{O}(10^{-4})$.

Example 5: Aeroassisted Orbital Transfer

Consider the following three-phase optimal control problem taken from Ref. [30]. Minimize the cost functional

$$J = \sum_{i=1}^{3} \|\Delta \mathbf{V}_i\| \tag{50}$$

subject to the dynamic constraints (that correspond to motion over a spherical non-rotating Earth) are modeled in spherical coordinates as

$$\begin{array}{ll}
\text{Phases 1 and 3:} & \text{Phases 2:} \\
\dot{r} = v\sin\gamma & \dot{r} = v\sin\gamma \\
\dot{\theta} = \dfrac{v\cos\gamma\cos\psi}{r\cos\phi} & \dot{\theta} = \dfrac{v\cos\gamma\cos\psi}{r\cos\phi} \\
\dot{\phi} = \dfrac{v\cos\gamma\cos\psi}{r} & \dot{\phi} = \dfrac{v\cos\gamma\cos\psi}{r} \\
\dot{v} = -D - g\sin\gamma & \dot{v} = -D - g\sin\gamma \\
\dot{\gamma} = -\dfrac{1}{v}\left(g - \dfrac{v^2}{r}\right)\cos\gamma & \dot{\gamma} = \dfrac{1}{v}\left[-\dfrac{qS}{m}u_2 - \left(g - \dfrac{v^2}{r}\right)\cos\gamma\right] \\
\dot{\psi} = -\dfrac{1}{v}\dfrac{v^2}{r}\cos\gamma\cos\psi\tan\phi & \dot{\psi} = -\dfrac{1}{v}\left[\dfrac{qS}{m\cos\gamma}u_1 + \dfrac{v^2}{r}\cos\gamma\cos\psi\tan\phi\right]
\end{array} \tag{51}$$

where r is the geocentric radius, θ is the longitude, ϕ is the geocentric latitude, v is the speed, γ is the flight path angle, ψ is the heading angle, $g = \mu/r^2$ is the gravitational acceleration, μ is the gravitational parameter, and $q = \rho v^2/2$ is the dynamic pressure. Phases 1 and 3 of this problem occur outside of the atmosphere while phase 2 occurs in the atmosphere. The impulses $\Delta\mathbf{V}_1 \in \mathbb{R}^3$, $\Delta\mathbf{V}_2 \in \mathbb{R}^3$, and $\Delta\mathbf{V}_3 \in \mathbb{R}^3$ are modeled in Earth-centered inertial (ECI) Cartesian coordinates and are applied at the beginning of Phase 1, the end of Phase 2, and the end of Phase 3. Each impulse is transformed to spherical coordinates via the transformation

$$\{\Delta\mathbf{V}\}_{sph} = T_e^s(\Delta\mathbf{V}) \tag{52}$$

where T_e^s is the nonlinear transformation from ECI to spherical coordinates (see Appendix). The first impulse de-orbits the vehicle into the atmosphere, the second impulse boosts the vehicle upon atmospheric exit, and the third impulse circularizes the vehicle into its final orbit. The controls during atmospheric flight are u_1 and u_2, defined as

$$\begin{aligned} u_1 &= -C_L \cos\sigma \\ u_2 &= -C_L \sin\sigma \end{aligned} \tag{53}$$

where σ is the bank angle. The controls u_1 and u_2 are constrained by the inequality path constraint

$$\sqrt{u_1^2 + u_2^2} \leq C_{L,\max} \tag{54}$$

where $C_{L,\max}$ is the maximum allowable coefficient of lift. It is noted that the bank angle can be computed from u_1 and u_2 as

$$\sigma = \tan^{-1}(u_1, u_2) \tag{55}$$

where $\tan^{-1}$ is the four-quadrant inverse tangent. The initial conditions correspond to an equatorial circular orbit of altitude h_0 and are given in terms of orbital elements as

$$\begin{aligned} a &= R_e + h_0 \quad , \quad e &= 0 \\ i &= 0 \text{ deg} \quad , \quad \Omega &= 0 \text{ deg} \\ \omega &= 0 \text{ deg} \quad , \quad \nu &= 0 \text{ deg} \end{aligned} \tag{56}$$

where a, e, i, Ω, ω, and ν are the semi-major axis, eccentricity, inclination, longitude of ascending node, argument of periapsis, and true anomaly, respectively [44], and R_e is the equatorial radius of the Earth. Next, the following inequality constraint is imposed at the terminus of Phase 2:

$$\gamma\left(t_f^{(2)}\right) \geq 0 \tag{57}$$

where $t_f^{(2)}$ is the time at the end of phase 2. Finally, a terminal constraint is placed on the inclination as

$$\cos i(t_f) = \cos\phi(t_f)\cos\gamma(t_f) \tag{58}$$

For this example we choose $i(t_f) = 10$ deg and a maximum lift coefficient $C_{L,\max} = 0.4$. The problem is solved using a canonical system of units where length is in units of Earth radii (R_e), time is in units of $\sqrt{\mu/R_e}$, speed is in units of $\sqrt{\mu/R_e}$, and mass is in units of initial spacecraft mass. Finally, it is noted that the mass drop across an impulse is taken into account by reducing the mass using the rocket equation

$$\|\Delta\mathbf{V}\| = g_0 I_{sp} \ln(m^+/m^-) \tag{59}$$

where m^+ and m^- are the values of the mass immediately before and application of the impulse, $\Delta\mathbf{V}$, and I_{sp} is the engine specific impulse. Thus, this example contains continuous variables (state and

control) along with the static optimization parameters $\Delta\mathbf{V}_1$, $\Delta\mathbf{V}_2$, $\Delta\mathbf{V}_3$, and the values of mass $m^{(1))}$, $m^{(2)}$, and $m^{(3)}$ that represent the mass during phases 1, 2, and 3.

The solution to the aeroassisted orbital transfer optimal control problem was obtained using the hp-adaptive pseudospectral method of Section 6 using $\rho = 3$, $\epsilon = 10^{-4}$ and an initialization of 10 collocation points per phase. In phases 1 and 3 single global segments of 10 collocation points each were obtained with a maximum value of Eq. (27) of $\mathcal{O}(10^{-11})$. Phase 2 consisted of seven segments each of 5 collocation points, except that the first and last segments of phase 2 have 15 collocation points. It was found that the maximum of Eq. (27) of the solution on the final grid in phase 2 is 8.66×10^{-5}.

The solution on the final grid in phase 2 (i.e., the atmospheric phase) is shown in Fig. 8. In this problem it is interesting to observe that the collocation points are densely located near the minimum altitude. The dynamics change most rapidly near the minimum altitude because the atmospheric force is the greatest in this region (thus providing the greatest lift on the vehicle anywhere on the trajectory). Consistent with this last observation, Fig. 8d shows that the bank angle changes most rapidly near minimum altitude. Finally, Fig. 8f shows the Hamiltonian, H, as a function of t. It is seen that the Hamiltonian is close to zero, as expected because the Hamiltonian is not an explicit function of time and the final time is free.

8 Discussion of Results

The results of Section 7 demonstrate several key features of the hp-adaptive pseudospectral method developed in this paper. Examples 1 is a problem with a nonsmooth optimal control where the hp-adaptive pseudospectral method is both more computationally efficient and more accurate than a global approach. In addition, the hp-adaptive solution contains many fewer total collocation points as compared with a global approach. Because the optimal control in Example 1 is non-smooth (in this case, discontinuous in the control), a global approximation was unable to provide a solution where tighter tolerances (e.g., 10^{-2}) were used. Also, it was found for this example that using Eq. 27 as a convergence criteria results in a very conservative approximation of the true accuracy in the state. The actual accuracy of the state on the final grid was one to two orders of magnitude greater than the maximum residual of Eq. (27).

In Example 2, the location of the segment breaks and allocation of collocation points changed as a function of the final time. Specifically, for this example the percentage of the solution in the "take-off" and "landing" decreases as t_f increases. For small to moderate values of t_f, a global approach was feasible for only loose accuracy tolerances. For larger values of t_f (e.g., $t_f = 5000$), the hp-adaptive method developed in this paper was computationally efficient and gave solutions to tighter

accuracy tolerances than global collocation. In the case of large t_f it was found that the placement of the collocation points was as expected, that is the hp-method placed a large number of collocation points in the "take-off" and "landing" segments (where the state and control change) and placed many fewer collocation points in the "cruise" segment. As t_f is increased further, greater computational resources were required but computationally efficient solutions were still obtained.

Examples 3 and 4 re-emphasize the increased accuracy and computational efficiency of the hp-adaptive pseudospectral method of this paper over global collocation. Example 4 demonstrates how the hp-method of this paper treats a problem with active inequality path constraints. Similar to the results of Examples 1, the hp-adaptive method is more efficient and accurate than a p-method. In this example, the p method did not converge for very loose accuracy tolerances. Interestingly, when the hp-adaptive method is used, the segments are divided near the activity/inactivity of the path constraint. In addition, many segments and collocation points were used to capture the ascent of the aircraft from the runway. In contrast, the final segment of the trajectory has significantly less interesting behavior and, thus, fewer collocation points and segments are used to approximate this section of the trajectory.

Example 5 shows the utility of the hp-adaptive method on a multiple-phase problem. In this example suitable solutions were found using a mixture of globally collocated phases (phases 1 and 3) and a phase that requires segmentation (phase 2). The key attribute of the hp-adaptive pseudospectral method for this example is that the collocation points were more densely located in the middle of the atmospheric phase. The behavior of the adaptive hp-adaptive pseudospectral method for Example 4 is similar to that of Example 2, i.e., the collocation points are located in regions where the greatest action takes place.

9 Possible Limitations of the hp-Adaptive Pseudospectral Method

While the hp-adaptive pseudospectral method developed in this paper has been found to be successful on a range of problems, it has some possible limitations that we now describe. First, in the approach developed in this paper, the mesh can only increase in size. For example, in Example 1 the method terminated using more segments than were theoretically necessary. If it was possible to decrease the number of collocation points or segments, the result might have been a three-segment solution with a short segment bracketing the control discontinuity. Ideally, two segments connected at the exact location of the discontinuity would be utilized. The inefficiency of terminating with six segments, while not significant in Example 1, might be important in other applications (e.g., a problem with a multiple bang-bang solution). Secondly, the method may have some difficulties on a problem with a very high frequency periodic solution. For such a problem, because the solution is smooth, the method may not divide the problem into segments. Instead, the method may simply increase without

bound the degree of a global polynomial approximation used. Finally, from our experience it typically takes many grid iterations when ϵ is small. Reducing the number of times the NLP solver is called would greatly increase the efficiency of this hp scheme.

10 Conclusions

An hp-adaptive pseudospectral method has been developed for solving optimal control problems. A strategy has been devised that determines the locations of segment breaks and the degree of the polynomial approximation required in each segment. The method has been applied to several examples of varying complexity. It has been found that the method produces solutions with better accuracy than global pseudospectral collocation while utilizing less computation time and resources. The method is demonstrated on a wide variety of applications ranging from problems with nonsmooth solutions to multiple-phase problems where the dynamics change more rapidly in certain regions of the trajectory than in other regions. The method has been integrated into a previously developed open-source pseudospectral optimal control software and is found to be a viable way to solve optimal control problems using pseudospectral methods.

Acknowledgments

The authors gratefully acknowledge support for this research from the National Science Foundation under Grant 0620286 and from the Florida Space Grant Consortium. It is noted that all examples and numerical data used to generate results in this paper have been obtained from the open literature.

Appendix: Transformation from ECI Cartesian to Spherical Coordinates

Consider a point in three-dimensional Euclidean space whose position (measured from the center of the Earth) and inertial velocity are modeled in Earth-centered inertial (ECI) Cartesian coordinates as $\mathbf{r} = (x, y, z)$ and $\mathbf{v} = (v_x, v_y, v_z)$. Let r, θ, ϕ, v, γ, and ψ be the geocentric radius, longitude, latitude, speed, flight path angle, and heading angle. Together $(r, \theta, \phi, v, \gamma, \psi)$ define a set of spherical coordinates. The transformation from ECI to spherical coordinates is given as follows. First, the radius and speed are computed as

$$\begin{aligned} r &= \|\mathbf{r}\|_2 = \sqrt{x^2 + y^2 + z^2} \\ v &= \|\mathbf{v}\|_2 = \sqrt{v_x^2 + v_y^2 + v_z^2} \end{aligned} \tag{60}$$

Next, the longitude and latitude are computed as

$$\begin{aligned} \theta &= \tan^{-1}(y, x) \\ \phi &= \tan^{-1}(z, \sqrt{x^2 + y^2}) \end{aligned} \tag{61}$$

where $\tan^{-1}(\cdot, \cdot)$ is the four-quadrant inverse tangent. Finally, the flight path angle and heading angle are computed as follows. First, let

$$\mathbf{e}_r = \mathbf{r}/r \quad , \quad \mathbf{e}_\theta = \frac{\mathbf{E}_z \times \mathbf{r}}{\|\mathbf{E}_z \times \mathbf{r}\|_2} \quad , \quad \mathbf{e}_\phi = \mathbf{e}_r \times \mathbf{e}_\theta \tag{62}$$

where $\mathbf{E}_z = \begin{bmatrix} 0 & 0 & 1 \end{bmatrix}^\mathsf{T}$. We then define the vector $\mathbf{v}_s$ as

$$\mathbf{v}_s = \begin{bmatrix} \mathbf{e}_r & \mathbf{e}_\theta & \mathbf{e}_\phi \end{bmatrix}^\mathsf{T} \mathbf{v} = \begin{bmatrix} v_r \\ v_\theta \\ v_\phi \end{bmatrix} \tag{63}$$

The flight path angle and heading angle are then computed as

$$\begin{aligned} \gamma &= \tan^{-1}(v_r, \sqrt{v_\theta^2 + v_\phi^2}) \\ \phi &= \tan^{-1}(v_\phi, v_\theta) \end{aligned} \tag{64}$$

References

1. Betts, J. T., *Practical Methods for Optimal Control Using Nonlinear Programming*, SIAM Press, Philadelphia, 2001.

2. Jain, D. and Tsiotras, P., "Trajectory Optimization Using Multiresolution Techniques," *Journal of Guidance, Control, and Dynamics*, Vol. 31, No. 5, September-October 2008, pp. 1424–1436.

3. Zhao, Y. and Tsiotras, P., "A Density-Function Based Mesh Refinement Algorithm for Solving Optimal Control Problems," Infotech and Aerospace Conference, AIAA Paper 2009-2019, Seattle, Washington, April 2009.

4. Betts, J. T. and Huffman, W. P., "Mesh Refinement in Direct Transcription Methods for Optimal Control," *Optimal Control Applications and Methods*, Vol. 19, 1998, pp. 1–21.

5. Cuthrell, J. E. and Biegler, L. T., "On the Optimization of Differential-Algebraic Processes," *AIChe Journal*, Vol. 33, No. 8, August 1987, pp. 1257–1270.

6. Cuthrell, J. E. and Biegler, L. T., "Simultaneous Optimization and Solution Methods for Batch Reactor Control Profiles," *Computers and Chemical Engineering*, Vol. 13, No. 1/2, 1989, pp. 49–62.

7. Elnagar, G., Kazemi, M., and Razzaghi, M., "The Pseudospectral Legendre Method for Discretizing Optimal Control Problems," *IEEE Transactions on Automatic Control*, Vol. 40, No. 10, 1995, pp. 1793–1796.

8. Elnagar, G. and Razzaghi, M., "A Collocation-Type Method for Linear Quadratic Optimal Control Problems," *Optimal Control Applications and Methods*, Vol. 18, No. 3, 1998, pp. 227–235.

9. Benson, D. A., *A Gauss Pseudospectral Transcription for Optimal Control*, Ph.D. thesis, Department of Aeronautics and Astronautics, Massachusetts Institute of Technology, Cambridge, Massachusetts, 2004.

10. Benson, D. A., Huntington, G. T., Thorvaldsen, T. P., and Rao, A. V., "Direct Trajectory Optimization and Costate Estimation via an Orthogonal Collocation Method," *Journal of Guidance, Control, and Dynamics*, Vol. 29, No. 6, November-December 2006, pp. 1435–1440.

11. Huntington, G. T., *Advancement and Analysis of a Gauss Pseudospectral Transcription for Optimal Control*, Ph.D. thesis, Massachusetts Institute of Technology, Cambridge, Massachusetts, 2007.

12. Rao, A. V., Benson, D. A., Darby, C. L., Francolin, C., Patterson, M. A., Sanders, I., and Huntington, G. T., "Algorithm: GPOPS, A Matlab Software for Solving Multiple-Phase Optimal Control Problems Using the Gauss Pseudospectral Method," *ACM Transactions on Mathematical Software*, Accepted for Publication, June 2009.

13. Rao, A. V., Benson, D. A., Darby, C. L., Patterson, M. A., Sanders, I., and Huntington, G. T., *User's Manual for* GPOPS *Version 2.2*, http://gpops.sourceforge.net/, June 2009.

14. Kameswaran, S. and Biegler, L. T., "Convergence Rates for Direct Transcription of Optimal Control Problems Using Collocation at Radau Points," *Computational Optimization and Applications*, Vol. 41, No. 1, 2008, pp. 81–126.

15. Garg, D., Patterson, M. A., Darby, C. L., Francolin, C., Huntington, G. T., Hager, W. W., and Rao, A. V., "Direct Trajectory Optimization and Costate Estimation of Finite-Horizon and Infinite-Horizon Optimal Control Problems via a Radau Pseudospectral Method," *Computational Optimization and Applications*, Published Online: October 6, 2009. DOI 10.1007/s10589-009-9291-0. http://www.springerlink.com/content/n851q6n343p9k60k/.

16. Garg, D., Patterson, M. A., Hager, W. W., Rao, A. V., Benson, D. A., and Huntington, G. T., "A Unified Framework for the Numerical Solution of Optimal Control Problems Using Pseudospectral Methods," *Automatica*, Provisionally Accepted for Publication December 2009. Current manuscript available at http://vdol.mae.ufl.edu/unifiedFramework.pdf.

17. Canuto, C., Hussaini, M. Y., Quarteroni, A., and Zang, T. A., *Spectral Methods in Fluid Dynamics*, Spinger-Verlag, Heidelberg, Germany, 1988.

18. Fornberg, B., *A Practical Guide to Pseudospectral Methods*, Cambridge University Press, 1998.

19. Trefethen, L. N., *Spectral Methods Using MATLAB*, SIAM Press, Philadelphia, 2000.

20. Babuska, I. and Suri, M., "The p and hp Version of the Finite Element Method, an Overview," *Computer Methods in Applied Mechanics and Engineering*, Vol. 80, 1990, pp. 5–26.

21. Babuska, I. and Suri, M., "The p and hp Version of the Finite Element Method, Basic Principles and Properties," *SIAM Review*, Vol. 36, 1994, pp. 578–632.

22. Gui, W. and Babuska, I., "The h, p, and hp Versions of the Finite Element Method in 1 Dimension. Part I. The Error Analysis of the p Version," *Numerische Mathematik*, Vol. 49, 1986, pp. 577–612.

23. Gui, W. and Babuska, I., "The h, p, and hp Versions of the Finite Element Method in 1 Dimension. Part II. The Error Analysis of the h and $h-p$ Versions," *Numerische Mathematik*, Vol. 49, 1986, pp. 613–657.

24. Gui, W. and Babuska, I., "The h, p, and hp Versions of the Finite Element Method in 1 Dimension. Part III. The Adaptive $h - p$ Version," *Numerische Mathematik*, Vol. 49, 1986, pp. 659–683.

25. Galvao, A., Gerritsma, M., and Maerschalk, B. D., "hp-Adaptive Least-Squares Spectral Element Method for Hyperbolic Partial Differential Equations," *Journal of Computational and Applied Mathematics*, Vol. 215, No. 2, June 2008, pp. 409–418.

26. Heinrichs, W., "An Adaptive least Squares Scheme for the Burgers Equation," *Numerical Algorithms*, Vol. 44, No. 1, January 2007, pp. 1–10.

27. Dorao, C. A. and Jakobsen, H. A., "hp-Adaptive Least Squares Spectral Element Method for Population Balance Equations," *Applied Numerical Mathematics*, Vol. 58, No. 5, May 2008, pp. 563–576.

28. Dorao, C. A., Fernandino, M., Jakobsen, H. A., and Svendsen, H. F., "hp-Adaptive Spectral Element Solver for Reactor Modeling," *Chemical Engineering Science*, Vol. 64, No. 5, March 2009, pp. 904–911.

29. Karniadakis, G. and Sherwin, S., *Spectral/hp Element Methods for CFD*, Oxford University Press, Oxford, UK, 1999.

30. Rao, A. V., Scherich, A. E., Cox, S., and Mosher, T. E., "A Concept for Operationally Responsive Space Mission Planning Using Aeroassisted Orbital Transfer," *2008 Responsive Space Conference*, AIAA Paper RS6-2008-7309, Los Angeles, California, April 2008.

31. Davis, P. J. and Rabinowitz, P., *Methods of Numerical Integration*, Academic Press, New York, 1984.

32. Abramowitz, M. and Stegun, I., *Handbook of Mathematical Functions with Formulas, Graphs, and Mathematical Tables*, Dover Publications, New York, 1965.

33. von Winckel, G., *collocD: Pseudospectral Differentiation on an Arbitrary Grid*, The Mathworks, Inc., Central File Exchange, July 2004.

34. Gill, P. E., Murray, W., and Saunders, M. A., *User's Guide for SNOPT Version 7: Software for Large Scale Nonlinear Programming*, February 2006.

35. Meditch, J., "On the Problem of Optimal Thrust Programming for a Soft Lunar Landing," *IEEE Transaction on Automatic Control*, Vol. 9, No. 4, 1964, pp. 477–484.

36. Rao, A. V. and Mease, K. D., "Dichotomic Basis Approach to solving Hyper-Sensitive Optimal Control Problems," *Automatica*, Vol. 35, No. 4, April 1999, pp. 633–642.

37. Rao, A. V. and Mease, K. D., "Eigenvector Approximate Dichotomic Basis Method for Solving Hyper-Sensitive optimal Control Problems," *Optimal Control Applications and Methods*, Vol. 21, No. 1, January–February 2000, pp. 1–19.

38. Rao, A. V., "Application of a Dichotomic Basis Method to Performance Optimization of Supersonic Aircraft," *Journal of Guidance, Control, and Dynamics*, Vol. 23, No. 3, May–June 2000, pp. 570–573.

39. Rao, A. V., "Riccati Dichotomic Basis Method for solving Hyper-Sensitive optimal Control Problems," *Journal of Guidance, Control, and Dynamics*, Vol. 26, No. 1, January–February 2003, pp. 185–189.

40. Betts, J. T. and Huffman, W. P., "Sparse Optimal Control Software – SOCS," Tech. Rep. MEA-LR-085, Boeing Information and Support Services, Seattle, Washington, July 1997.

41. Zhao, Y. J., "Optimal Pattern of Glider Dynamic Soaring," *Optimal Control Applications and Methods*, Vol. 25, 2004, pp. 67–89.

42. Bryson, A. E., Desai, M. N., and Hoffman, W. C., "Energy-State Approximation in Performance Optimization of Supersonic Aircraft," *AIAA Journal of Aircraft*, Vol. 6, No. 6, 1969, pp. 481–488.

43. Seywald, H. and Kumar, R. R., "Finite Difference Scheme for Automatic Costate Calculation," *Journal of Guidance, Control, and Dynamics*, Vol. 19, No. 4, 1996, pp. 231–239.

44. Bate, R. R., Mueller, D. D., and White, J. E., *Fundamentals of Astrodynamics*, Dover Publications, 1971.

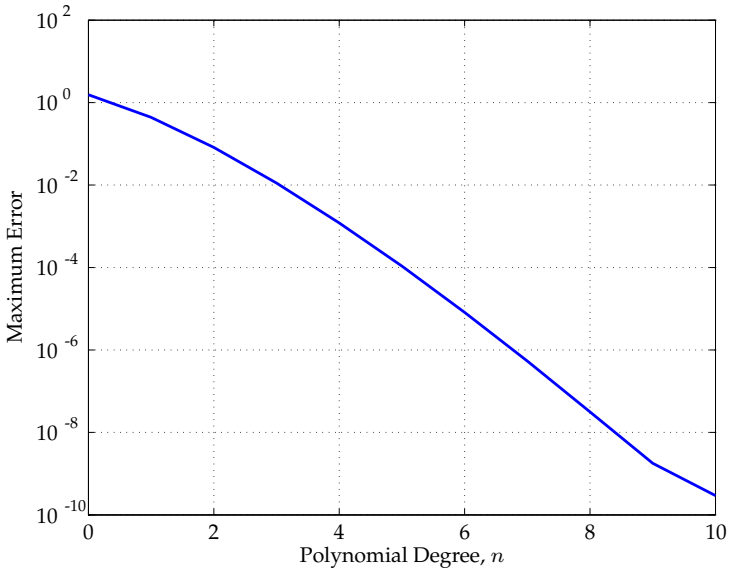

(a) Logarithm of Global Polynomial Maximum Least-Squares Error as a Function of Polynomial Degree for the Smooth Function in Eq. (1).

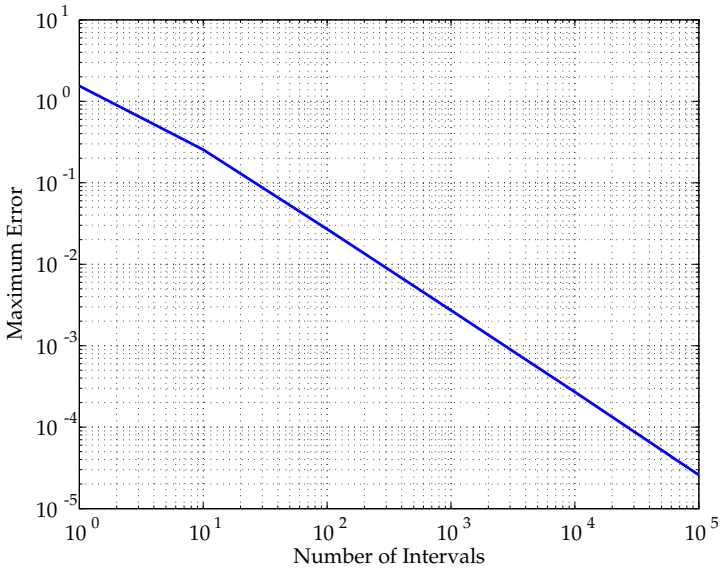

(b) Logarithm of Maximum Piecewise Constant Least-Squares Error as a Function of the Logarithm of the Number of Segments for the Smooth Function in Eq. (1).

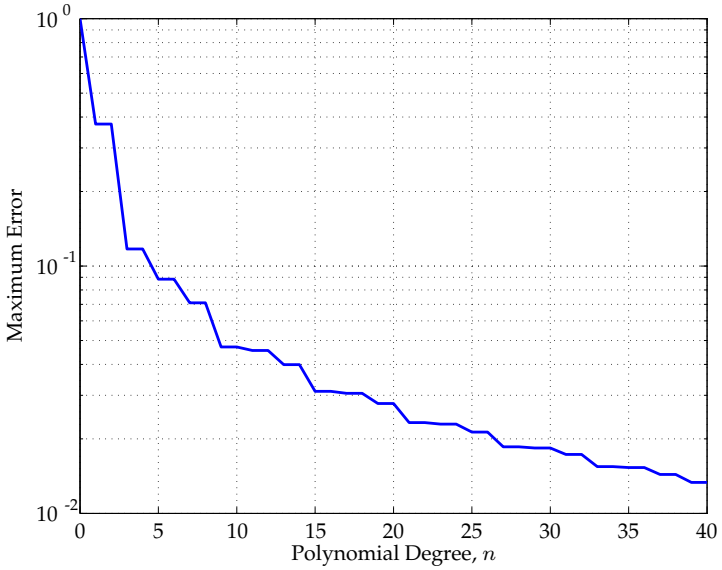

(c) Logarithm of Global Polynomial Maximum Least-Squares Error as a Function of Polynomial Degree for the Piecewise Smooth Function in Eq. (2).

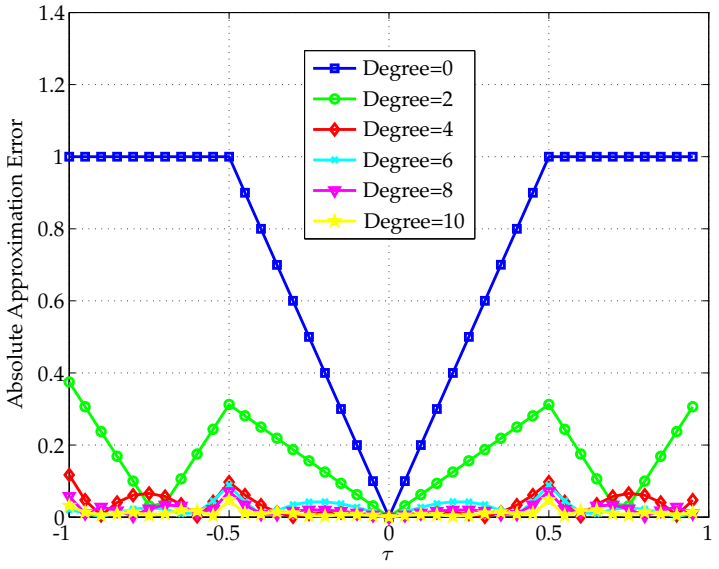

(d) Least-Squares Error as a Function of τ for Various Polynomial Degrees for Function in Eq. (2).

Figure 1: Least-Squares Errors Function Approximations for the Functions in Eqs. (1) and (2).

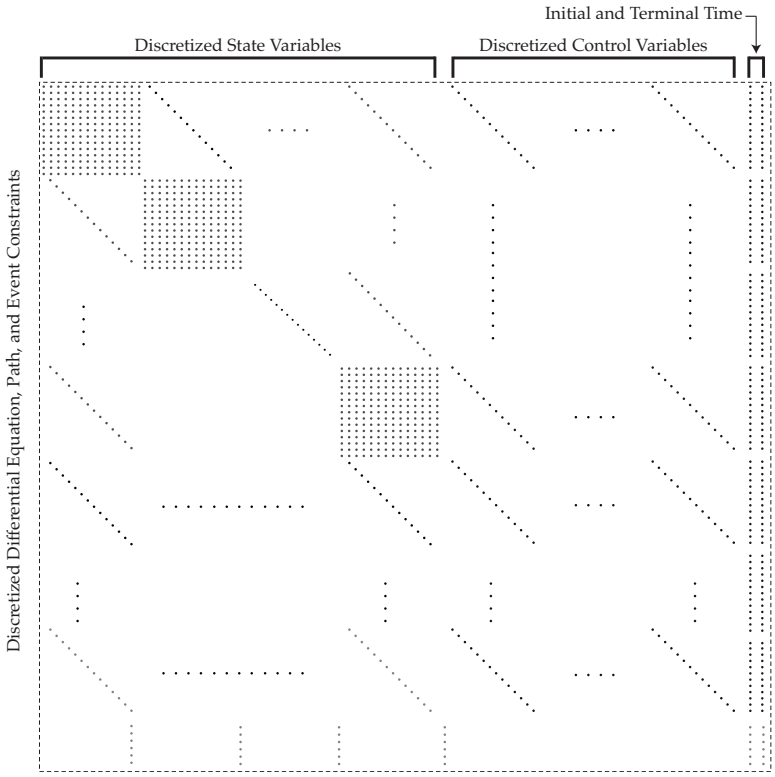

(a) Global Collocation.

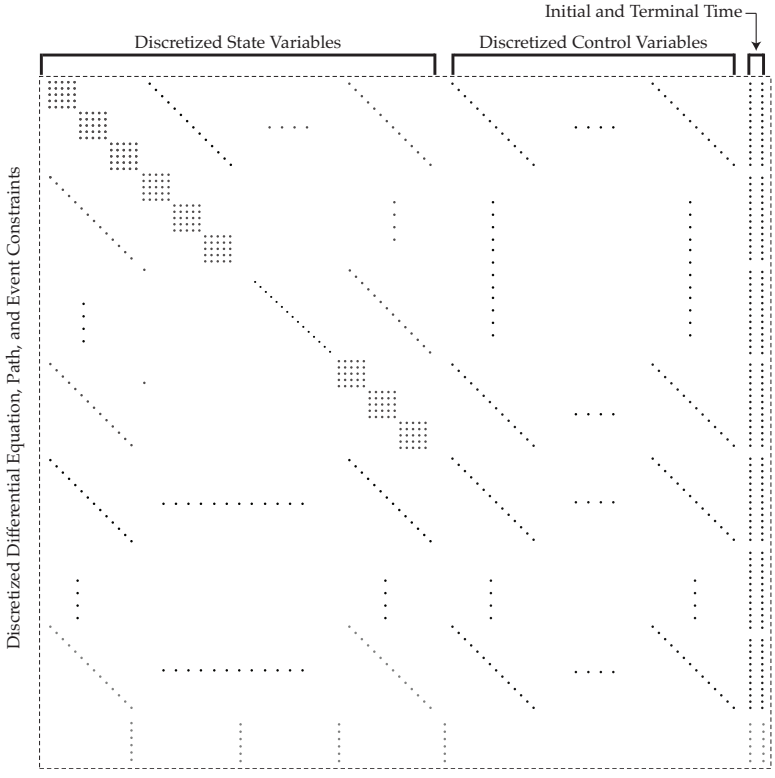

(b) Segmented Collocation.

Figure 2: Qualitative View of Constraint Jacobian Sparsity Pattern for a Pseudospectral Method Using Global and Segmented Collocation.

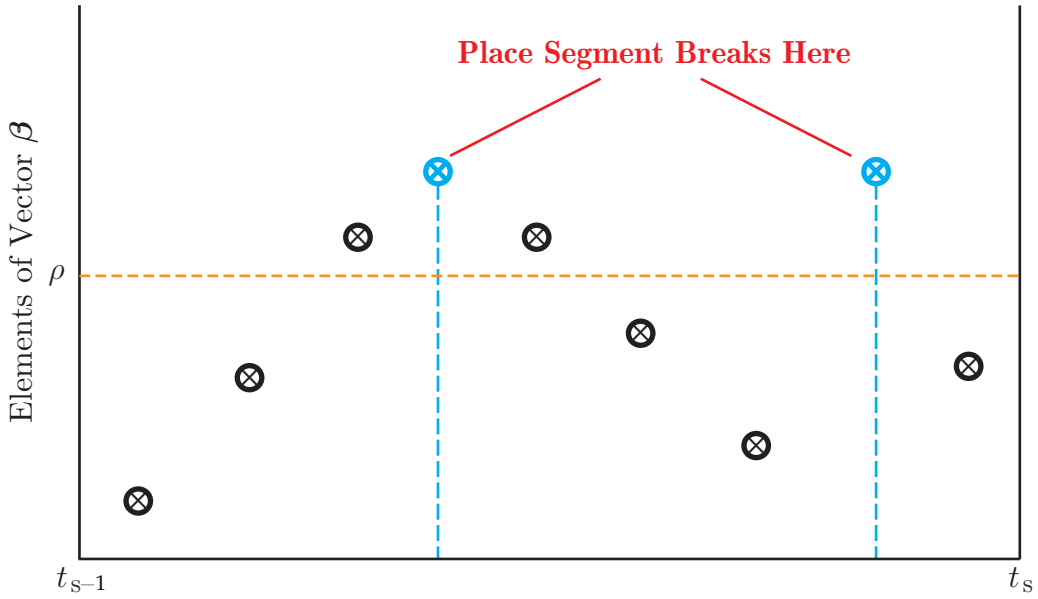

Figure 3: Schematic Showing The Strategy to Determine if a Trajectory Segment Needs to be Divided into More Segments and Where to Place the Segment Breaks.

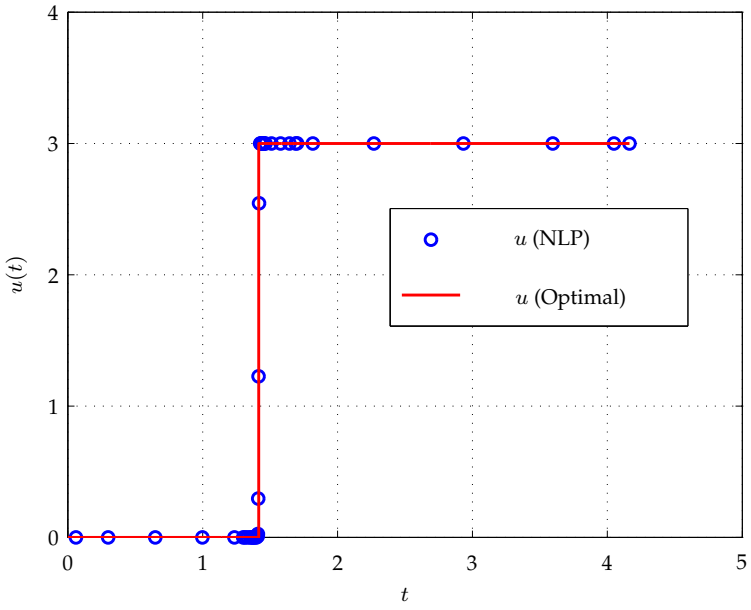

(a) Control vs. Time on Final Grid.

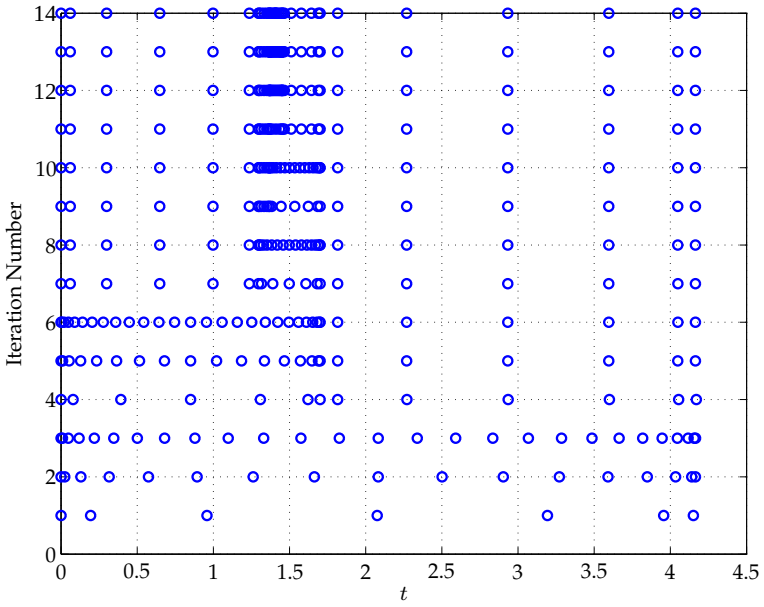

(b) State Approximation Points on Various Grids.

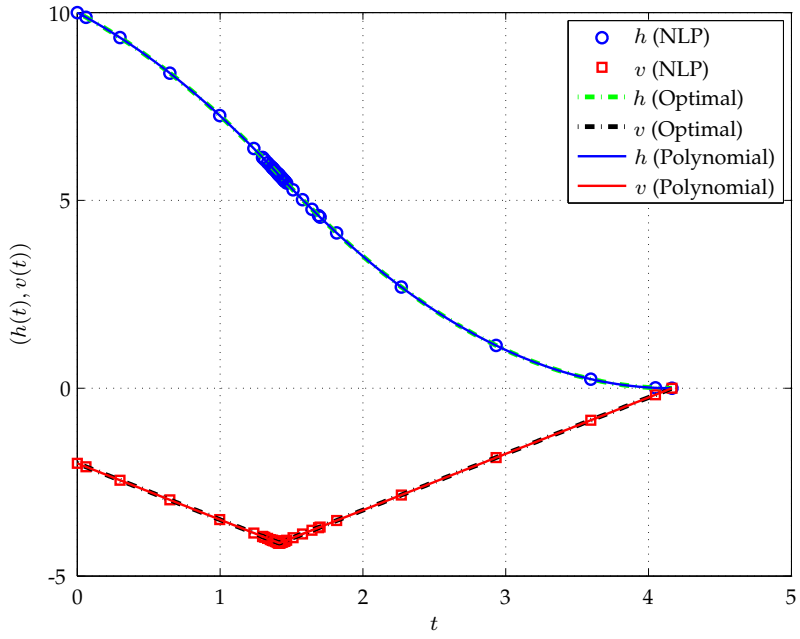

(c) State vs. Time on Final Grid.

Figure 4: Control and State on Final Grid and State Approximation Points (i.e., LG Points Plus Endpoints) on the Various Grids for Example 1.

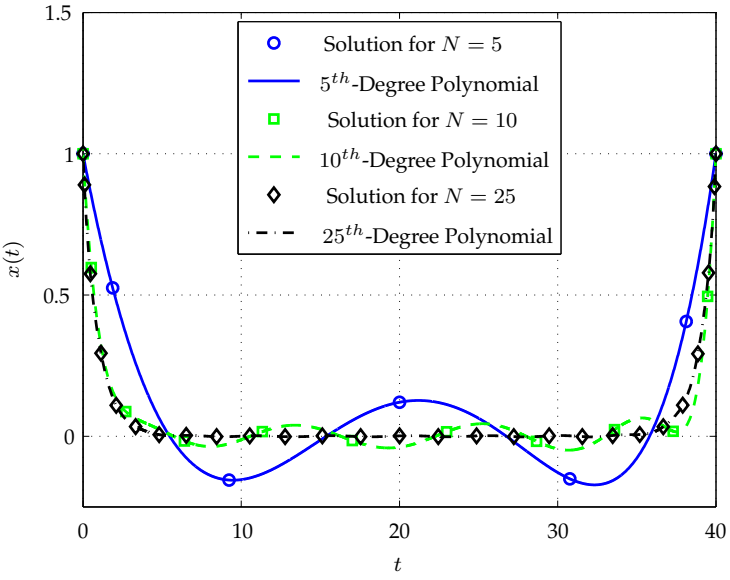

(a) Globally Collocated Solution for Various Values of N.

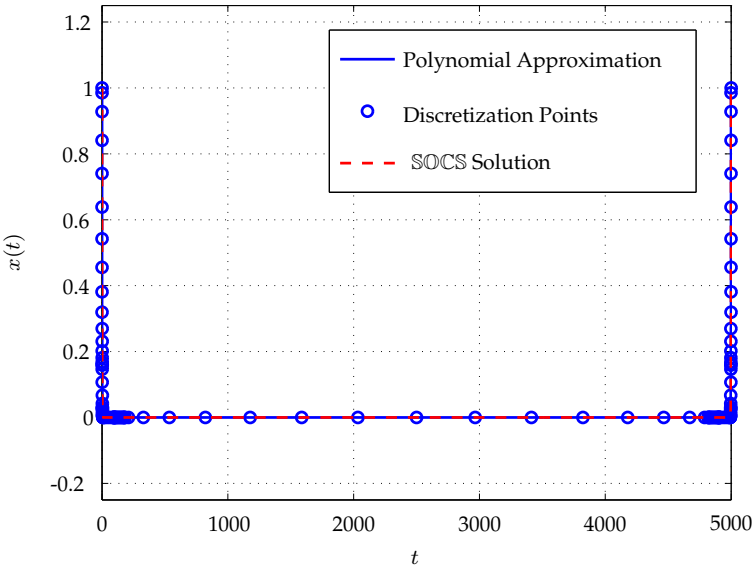

(b) Entire State Solution.

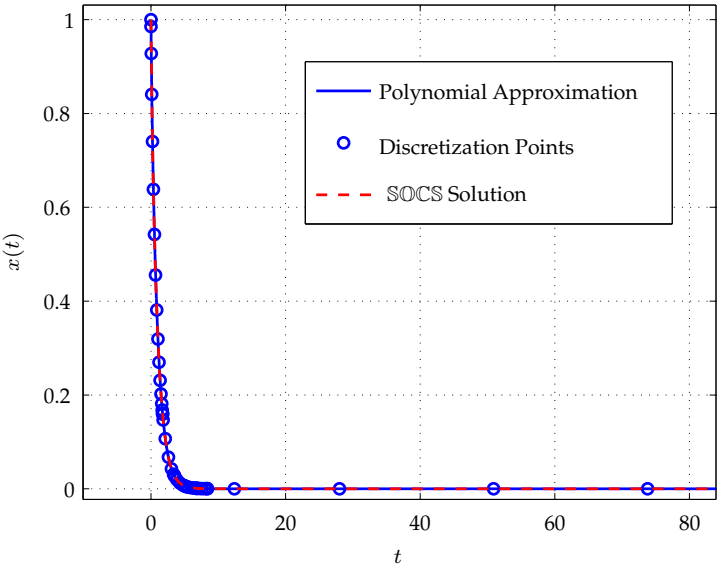

(c) Take-Off Segment.

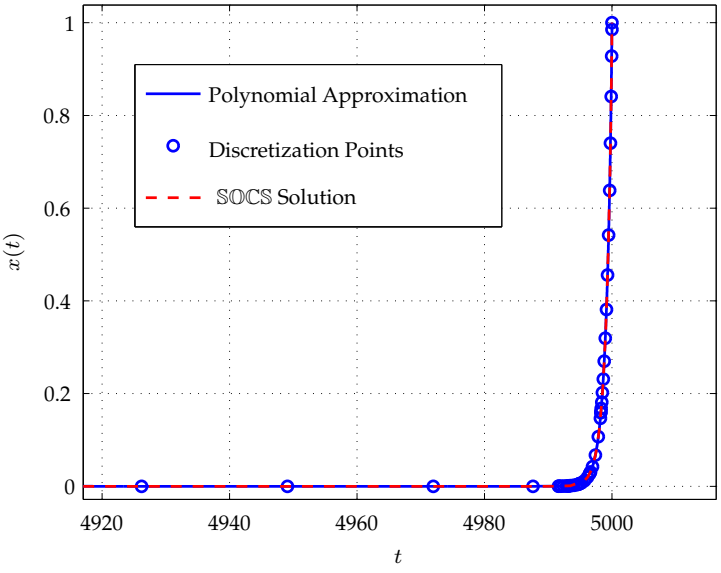

(d) Landing Segment.

Figure 5: State Solution for Example 2 with $t_f = 40$ Using Global Collocation and $t_f = 5000$ Using *hp*-Adaptive Pseudospectral Method.

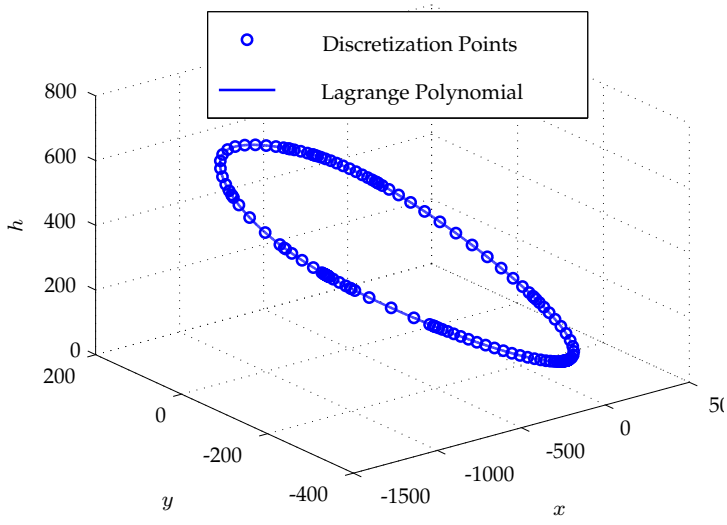

(a) Three-Dimensional Plot of (x, y, h).

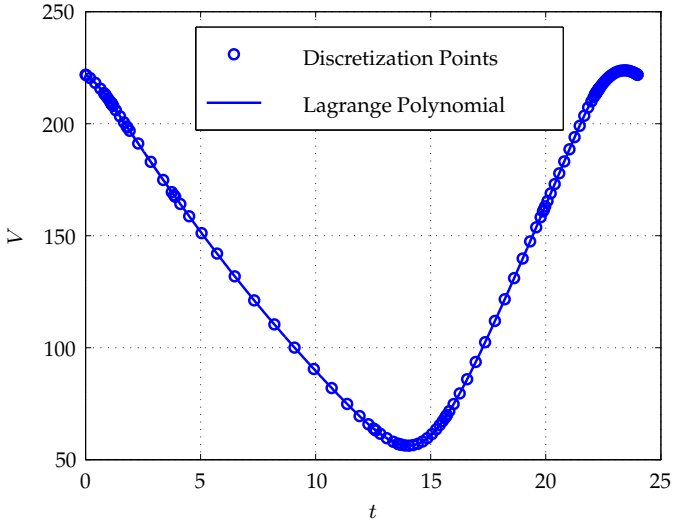

(b) V vs. t.

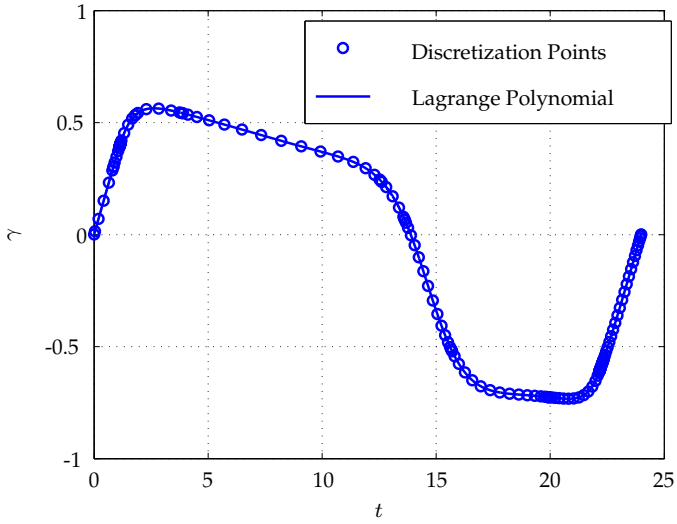

(c) γ vs. t.

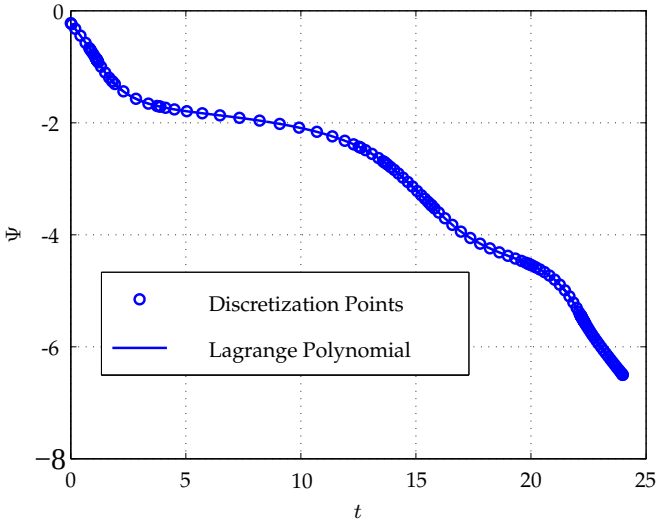

(d) Ψ vs. t.

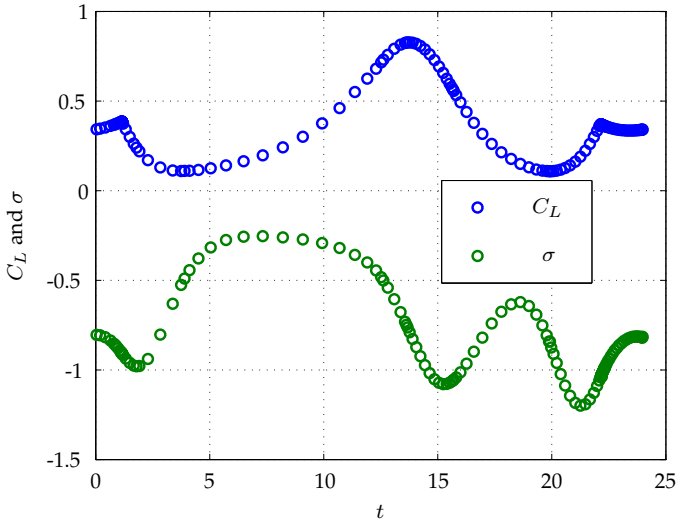

(e) C_L and μ vs. t.

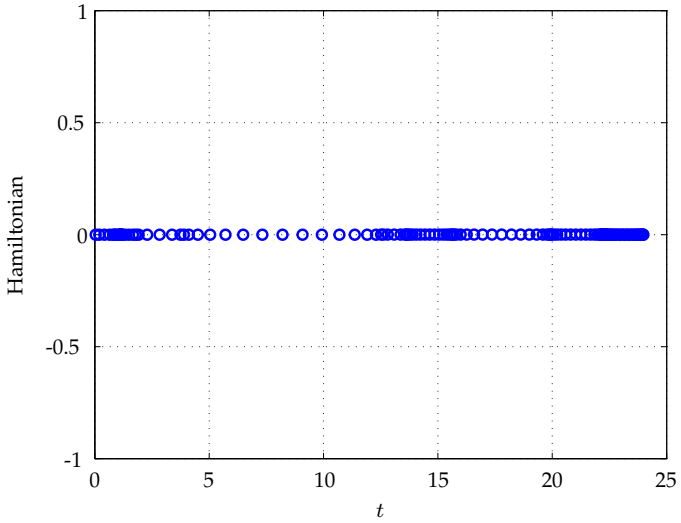

(f) Hamiltonian vs. t.

Figure 6: Solution on Final Grid for Example 3.

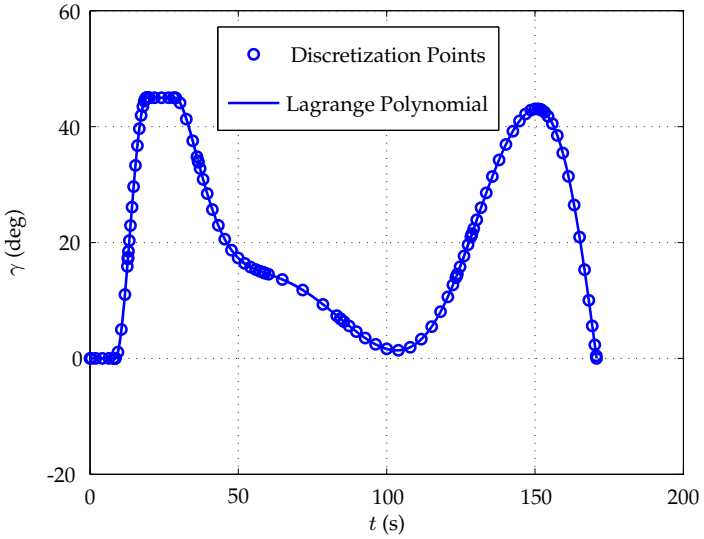

(a) Flight Path Angle vs. Time.

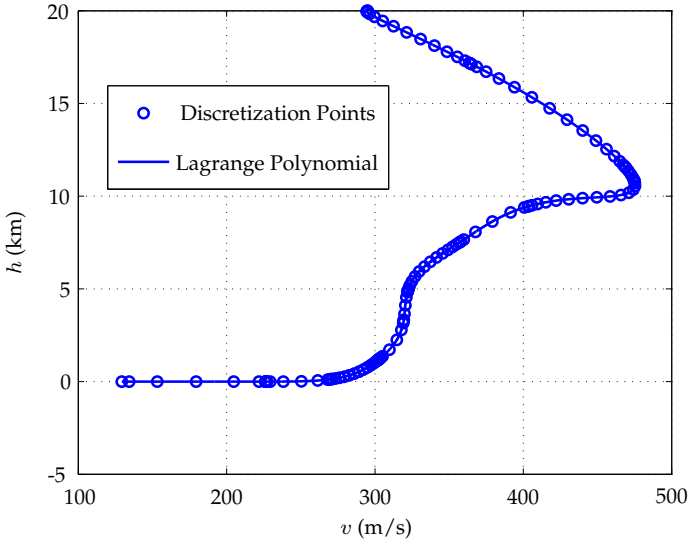

(b) Altitude vs. Speed.

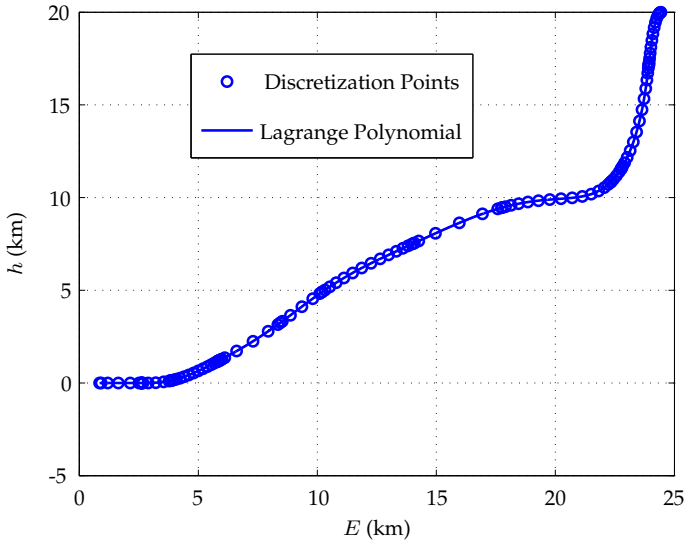

(c) Altitude vs. Energy Height.

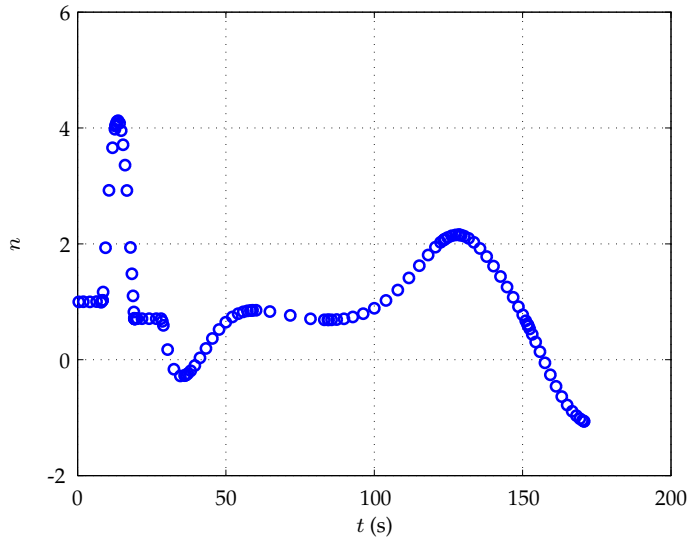

(d) Load Factor vs. Time.

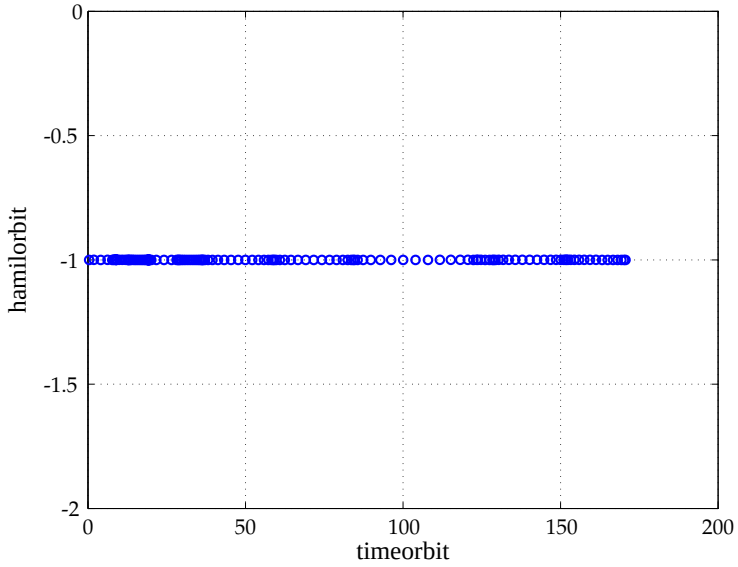

(e) Hamiltonian vs. t.

Figure 7: Solution for Example 4 on Final Grid.

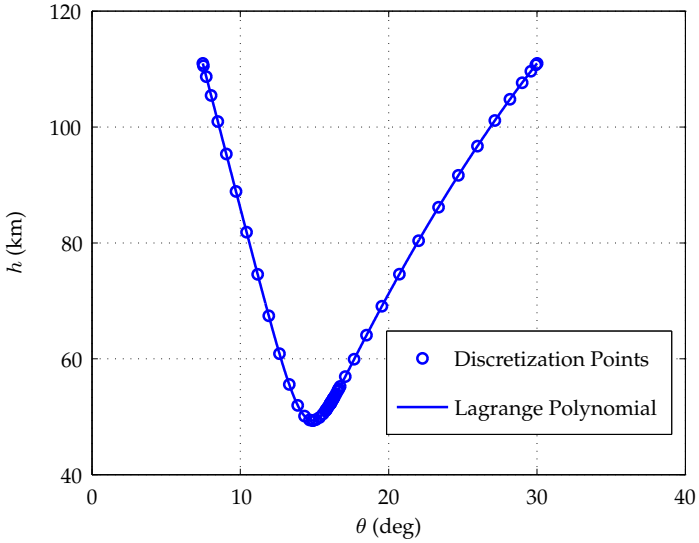

(a) Altitude vs. Longitude.

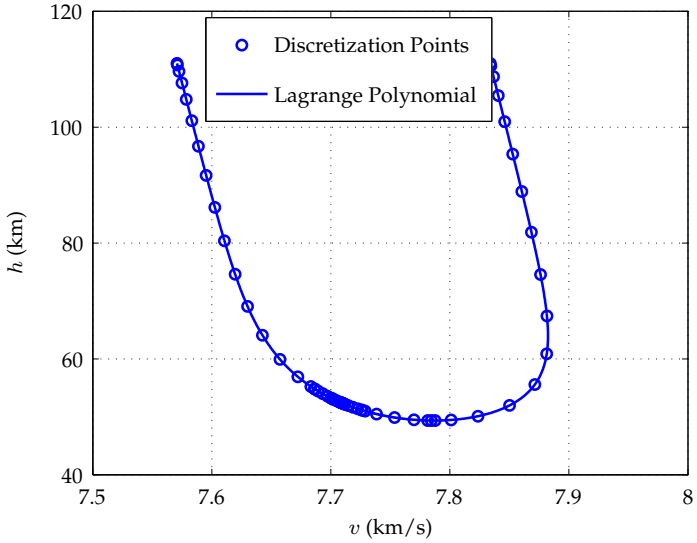

(b) Altitude vs. Speed.

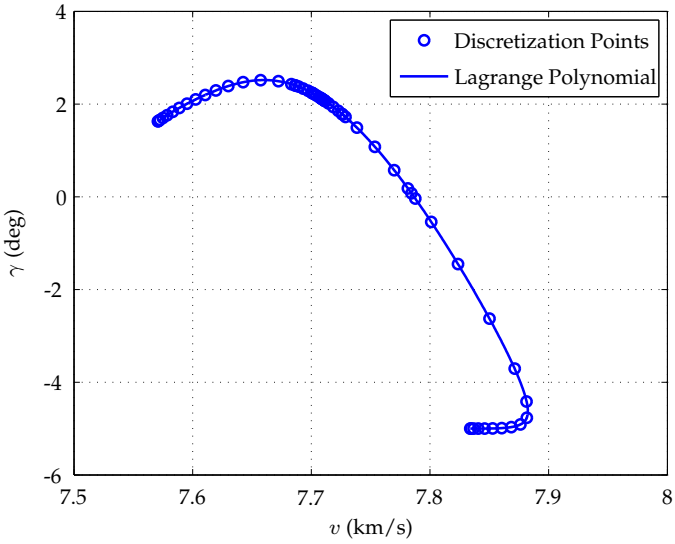

(c) Flight Path Angle vs. Speed

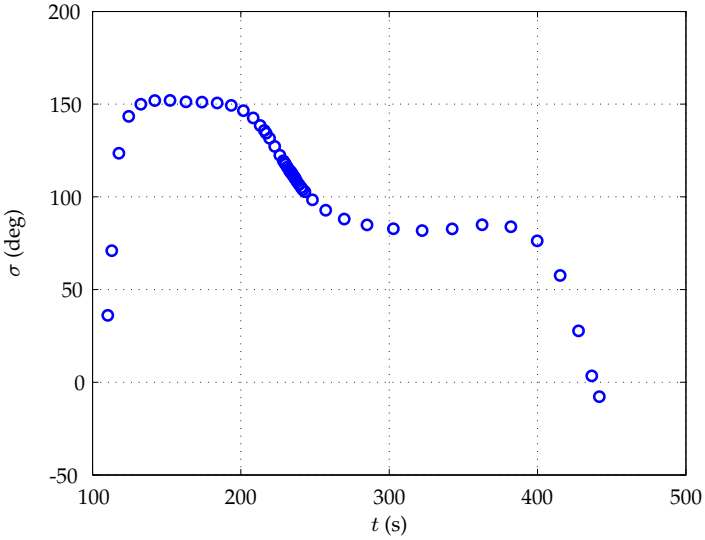

(d) Bank Angle vs. Time.

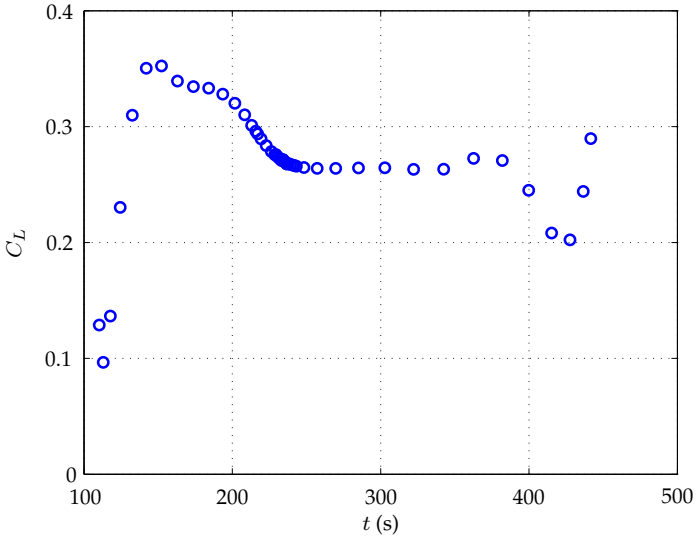

(e) Coefficient of Lift vs. Time.

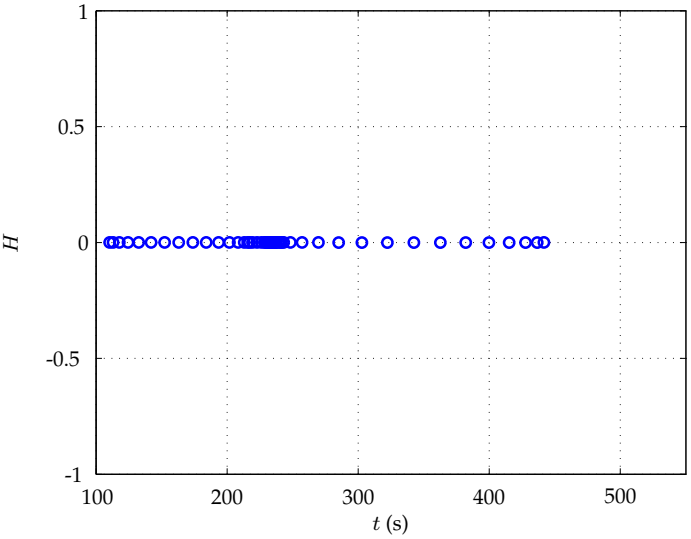

(f) Hamiltonian vs. Time.

Figure 8: Solution of Example 5 in Phase 2 on Final Grid.

ϵ	ρ	CPU Time (s)	Collocation Points	Segments	# of Grids	Max Infeasibility	Maximum Relative Error
10^{0}	Global	0.23	5	1	1	9.5×10^{-1}	5×10^{-2}
5×10^{-1}	Global	1.99	65	1	7	4.5×10^{-1}	2.5×10^{-1}
10^{-1}	Global	–	–	–	–	–	–
10^{-1}	3	0.89	10	2	4	7.3×10^{-2}	1.33×10^{-3}
10^{-2}	3	2.4	45	5	13	8.1×10^{-3}	8.43×10^{-5}
10^{-3}	3	3.21	40	6	15	8.2×10^{-4}	5.0×10^{-6}
10^{-4}	3	3.71	45	7	17	3.1×10^{-5}	1.82×10^{-6}
–	Global	13.41	200	1	1	5.94×10^{-1}	9.03×10^{-4}

Table 1: Summary of Accuracy and Speed Using the hp-Adaptive Pseudospectral Method for Example 1 Using Various Accuracy Tolerances, ϵ, and Global/Local Threshold Tolerances, ρ.

t_f	ϵ	CPU Time (s)	Collocation Points	# of Grids	Jacobian Density	Jacobian Entries
40	10^{-2}	2.35	105	11	50	11556
200	10^{-1}	20.3	175	18	50	31506
1000	10^{-1}	–	–	–	-	–

Table 2: Computational Performance of Global Collocation for Example 2.

t_f	ϵ	CPU Time (s)	Collocation Points	Segments	# of Grids	Jacobian Density	Jacobian Entries
40	10^{-3}	12.47	85	7	13	10.8	1830
200	10^{-3}	9.79	70	10	12	8.3	1042
1000	10^{-3}	14.24	120	16	14	5.22	1866
2000	10^{-3}	24.15	140	20	18	4.24	2082
5000	10^{-3}	19.93	135	17	13	4.85	2170

Table 3: Computational Performance of the hp-Adaptive Pseudospectral Method for Example 2 Using $\rho = 3$.

ϵ	ρ	CPU Time (s)	Collocation Points	Segments	Grid Iterations	Jacobian Density	Jacobian Entries
10^{-1}	Global	25.6	50	1	5	12.8	19215
5×10^{-2}	Global	68.6	90	1	9	11.9	56135
10^{-2}	Global	—	—	—	—	—	
10^{-1}	3	26.1	30	4	7	6.8	4409
10^{-2}	3	84.4	65	75	9	2.8	13085
10^{-3}	3	300.8	155	13	14	1.8	30113

Table 4: Summary of Accuracy and Speed Using the hp-Adaptive Pseudospectral Method for Example 3 Using Various Accuracy Tolerances, ϵ.

ϵ	ρ	CPU Time (s)	Collocation Points	Segments	# of Grids	Jacobian Density	Jacobian Entries
10^{0}	Global	–	–	–	–	–	–
10^{-1}	3	10.34	30	4	5	10.5	1856
10^{-2}	3	21.47	75	6	8	6.1	5804
10^{-3}	3	36.68	120	14	12	3.0	7796
10^{-4}	3	119.78	260	34	19	1.3	16196

Table 5: Summary of Computational Performance of the hp-Adaptive Pseudospectral Method for Example 4 Using Various Values of ϵ and ρ.